vibration

MDPI

Article

Transfer Learning Approach for Estimating Modal Parameters of Robot Manipulators Using Minimal Experimental Data

Seyed Hamed Seyed Hosseini [1,2], Seyedhossein Hajzargarbashi [2,*], Gabriel Côté [2] and Zhaoheng Liu [1]

[1] Department of Mechanical Engineering, École de Technologie Supérieure, Université du Québec, 1100 Notre-Dame St W, Montreal, QC H3C 1K3, Canada; seyed-hamed.seyed-hosseini.1@ens.etsmtl.ca (S.H.S.H.); zhaoheng.liu@etsmtl.ca (Z.L.)

[2] Aerospace Manufacturing Technologies Centre, National Research Council Canada, 2107 Chemin de Polytechnique, Montreal, QC H3T 1J4, Canada; gabriel.cote@cnrc-nrc.gc.ca

* Correspondence: seyedhossein.hajzargarbashi@cnrc-nrc.gc.ca

Abstract

Robots are used more and more in manufacturing, especially in tasks like robotic machining, where understanding their vibration behavior is very important. However, robot vibrations vary with posture, and evaluating all representative postures requires significant time and cost. This study proposes a deep learning (DL) based transfer learning (TL) approach to predict robot vibration behavior using fewer experiments. A large dataset was collected from a KUKA KR300 robot (Robot A) by testing nearly 250 postures. This dataset was then used to train a model to predict modal parameters such as natural frequencies (ω_n), damping ratios (ξ), and modal stiffness (k) within the workspace. TL was then used to apply the knowledge from Robot A to two other robots: a Comau NJ 650-2.7 (Robot B, high-payload) and an ABB IRB 4400 (Robot C, low-payload). Only a small number of postures were tested for Robots B and C. They were chosen carefully to cover different workspace areas and avoid collisions. Hammer tests were performed, and a four-step process was used to identify the real vibration modes. Stabilization diagrams were applied to confirm valid modes and remove noise. The results show that TL can accurately predict modal parameters for both Robot B and Robot C, even with limited data. These predictions were also used to estimate frequency response functions (FRFs), which matched well with experimental results. The main novelties of this work are: achieving accurate prediction of posture-dependent dynamics using minimal experimental data, demonstrating generalization across robots with different payload capacities, and revealing that data coverage across the workspace is more critical than dataset size.

Keywords: robot machining; modal parameter identification; transfer learning (TL); vibration analysis; frequency response function (FRF)

Academic Editor: Maria Chierichetti

Received: 28 August 2025
Revised: 7 October 2025
Accepted: 14 October 2025
Published: 18 October 2025

Citation: Seyed Hosseini, S.H.; Hajzargarbashi, S.; Côté, G.; Liu, Z. Transfer Learning Approach for Estimating Modal Parameters of Robot Manipulators Using Minimal Experimental Data. *Vibration* **2025**, *8*, 65. https://doi.org/10.3390/vibration8040065

1. Introduction

Industrial robotic manipulators are widely used in manufacturing, aerospace, healthcare, and logistics for tasks such as assembly, machining, inspection, and material handling. In these applications, positioning accuracy, path repeatability, and dynamic stability are critical. A persistent obstacle to high performance is vibration: structural flexibility in long links, gear train compliance, and controller bandwidth limitations can excite modes that reduce accuracy, degrade surface finish, and limit process productivity [1]. To understand and control these effects, engineers rely on modal parameters including natural

frequencies, damping ratios, and modal stiffness, as well as the frequency response function (FRF), which characterizes how a robot responds to harmonic excitations across a range of frequencies. However, measuring posture-dependent modal parameters and FRFs requires extensive and costly experimental tests (hammer or shaker tests across many joint configurations) and/or time-consuming modeling activities (finite element models and parameter tuning). Such intensive testing and modeling requirements make it difficult to maintain accurate, up-to-date dynamic maps of large workspaces, especially for high-payload, long-reach robots used in machining.

Recent works have explored data-driven methods to reduce this burden. Machine learning (ML) and deep learning models can learn complex input–output relations from data and have been used in robotics for quality inspection, fault detection, path planning, and adaptive control, often improving robustness and decision-making in changing environments [2–4]. For example, Mendez et al. [5] reported high task accuracy in collaborative assembly using deep networks; Adebayo et al. [6] and Agrawal et al. [7] documented the use of computer vision and predictive maintenance for defect detection and failure prognosis. Singh et al. [8] showed ML-assisted material handling in dynamic factory layouts, and Huang et al. [9] highlighted the synergy between digital twins and ML for real-time monitoring. Reinforcement learning has also enabled force-sensitive tasks such as deburring and polishing [10]. In parallel, ML has been applied to vibration analysis, including ANN-based identification, chatter detection, and dynamic parameter estimation [11–13]. While promising, most of these studies require large labeled datasets gathered on a single robot or within a narrow operating window. The data requirements and retraining effort remain barriers when we need models that generalize across postures and, especially, across different robot platforms.

Transfer learning offers a principled way to reduce data requirements by reusing knowledge learned in a source setting to accelerate learning in a related target setting. The idea mirrors human learning, where prior knowledge transfers across tasks [14–16]. In robotics, transfer learning has been used to adapt skills across tasks, embodiments, and environments. Xiang et al. [17] proposed Diff-Transfer to leverage simulation as prior knowledge; Yang et al. [18] used generative models for cross-robot policy sharing; Chen et al. [19] adapted grasping skills across domains using visual cues; Monorchio et al. [20] exploited image features in collaborative robots; Sun [21] and Scheiderer [22] applied Progressive Neural Networks for faster reuse; and Guo et al. [23] decomposed complex motions into reusable primitives. Additional studies have bridged the simulation-to-reality gap using teacher–student schemes, domain adaptation, and safety-aware policy transfer [24–28]. Despite this progress, most prior work targets control and task execution. Far fewer studies use transfer learning to generalize vibration behavior (modal parameters and FRFs) across postures and robots, where the governing dynamics vary due to changes in joint angles, payloads, and end-effector conditions.

For vibration modeling, classical approaches—Experimental Modal Analysis (EMA), Finite Element Modeling (FEM), and Operational Modal Analysis (OMA)—remain foundational but can be expensive when applied over large posture grids [29]. Hybrid physics-based model and data-driven methods have been introduced to scale dynamical predictions, including digital twin frameworks to predict posture-dependent FRFs [30], multi-task Gaussian process regression for efficient FRF estimation [31], random-forest models for joint and cross-coupled modal behaviors [32], and Receptance Coupling Substructure Analysis (RCSA) for posture-aware FRF estimation [33]. Recent studies also examined the influence of tool–robot interface stiffness on FRFs [34] and evaluated experimental strategies for FRF estimation in 6-axis robots [35]. These advances are important for generating stability lobe diagrams used to avoid chatter and select productive cutting parameters in robotic

machining [36–39]. Nevertheless, maintaining accurate FRF maps across the workspace still requires significant data collection, highlighting the need for approaches capable of learning effectively from limited new measurements.

Transfer learning offers a direct solution to this challenge. In the inductive case, the source and target tasks share the same label space, but the target robot has very few labeled samples. In this setting, a model trained on one robot with a large dataset (source) can be adapted to another robot with only a few tests (target). Inductive transfer learning has demonstrated strong performance in many fields when labeled data are limited [40–42]. Other forms of transfer learning are transductive transfer (domain adaptation with unlabeled targets) and unsupervised transfer (no labels in either domain), which use methods such as representation alignment, self-supervision, or disentanglement to reduce inter-domain differences [43–51]. In industrial robots and machining, where performing extensive hammer tests for every robot and posture is impractical, inductive transfer learning is very useful. With a well-trained source model and a small number of labeled samples from the target, the model can be adapted to new robots and operating conditions with minimal additional effort.

Accurate FRFs are critical because stability lobe diagrams (SLDs), which guide chatter-free machining, are directly derived from the tool–point FRF. Changes in robot posture alter the FRF and therefore also shift the SLD. Previous studies have highlighted the dependence of SLDs on robot posture, configuration, and cutting conditions [37–39,52]. Machine learning has also been applied to predict chatter or learn SLDs [53–57]. Other approaches focused on in-process FRF prediction or combining static and motion-state FRFs for chatter control [58–63]. Our study extends these works by linking FRF prediction with transfer learning to enable posture-aware SLD construction for robots.

This paper develops a posture-aware method to model vibration and predict frequency response functions (FRFs) of high-payload and low-payload industrial robots used in machining. Using robot joint angles and a small set of hammer tests, we train deep models to estimate modal parameters (natural frequencies, damping ratios, and stiffness) and full FRFs. The model is first trained on a well-sampled reference robot (Robot A) and then adapted to other robots (Robots B and C) using transfer learning, reducing the need for large new datasets. The contribution of this work is indeed to provide reliable posture-dependent FRFs with fewer experiments, making SLD construction more efficient and practical for robotic machining.

1.1. Originality and Contribution of the Study

Prior ML studies in robotics have typically trained models separately for each robot, requiring large labeled datasets gathered through extensive testing at many postures [2–4,11–13]. In contrast, the originality of this work lies in an inductive transfer learning framework for posture-dependent vibration modeling and FRF prediction that reuses knowledge from one robot to another. We train a source model on Robot A with comprehensive hammer-test data and transfer it to Robots B and C using only limited labeled samples. This reduces experimental effort and cost while maintaining high prediction accuracy. The proposed approach is robot-agnostic (independent of the specific hardware of a robot) at the architecture level and requires only lightweight fine-tuning, making it suitable for deployment when new robots are introduced or when recalibration is needed after maintenance or payload changes.

The present work also provides a practical method for making vibration identification more data-efficient, including: (1) a posture sampling and testing plan designed to maximize information gained about the robot behaviour from each hammer test; (2) a model architecure that separates general knowledge from robot-specific calibration layers; and

(3) a validation protocol across different robots and dataset sizes to quantify the trade-off between accuracy and data use. Unlike earlier studies that focused on transferring control policies, adapting from simulation to reality, or task-level skills [17,18,21,23,27,64–68], our work is distinct in that it transfers vibration-related knowledge (modal parameters and FRFs) across robots. This contribution addresses a critical research gap and supports robotic stability analysis (via FRF-based SLDs), predictive maintenance.

1.2. Paper Organization

Section 2 describes the methodology, including the experimental design, hammer tests, data processing steps, and the deep learning framework with transfer learning. Section 3 presents and discusses the results, starting with modal prediction for Robot A, followed by transfer learning results for Robot B, and concluding with results for Robot C, where the effect of different training set sizes on prediction accuracy is analyzed. Finally, Section 4 summarizes the main findings and highlights the effectiveness of the proposed method in predicting modal parameters and estimating FRFs using limited data.

2. Methodology

In our previous work [69], a deep learning-based framework was presented to predict the modal parameters of a KUKA KR-300 robot manipulator (Robot A). Due to the posture-dependent nature of robot vibrations, an extensive experiment was carefully designed, comprising hammer tests in 254 robot configurations. Modal parameters in each robot configuration, including natural frequencies, damping ratios, and stiffnesses, were extracted to form a dataset. The challenges in selecting frequency peaks (modes) from FRF data during modal analysis and the proposed four-step method to accurately target them and extract modal parameters were explained in the reference [69]. The created dataset was used to train a feedforward neural network capable of accurately predicting these modal parameters in previously unseen robot configurations quickly. The predicted values were then used to estimate Frequency Response Functions (FRFs), which showed strong agreement with experimental results. A flowchart summarizing the complete methodology is presented in Figure 1, showing all steps from data acquisition to validation.

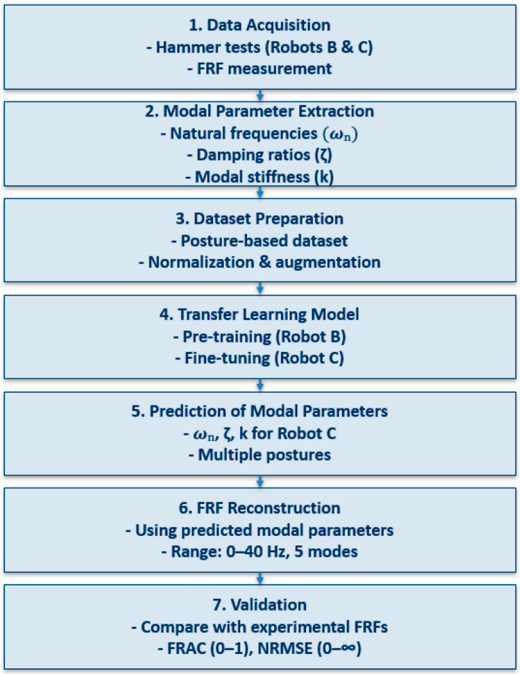

Figure 1. Flowchart of the proposed methodology for predicting robot modal parameters and FRFs.

In this section, only the methodology regarding the application of transfer learning based on the pretrained neural networks of Robot A is discussed. The setup, data collection and modal parameter extraction processes for Robot B (Comau, high-payload) and Robot C (ABB, low-payload) are the same as discussed in [69]. The pretrained model was then used to train new modal parameter prediction models for Robot B and Robot C, using significantly smaller datasets. The predicted modal parameters are then used to estimate the FRFs of Robots B and C and compared with the measured FRFs.

2.1. Experimental Design, Hammer Tests and Data Processing

The three robots selected for this study were KUKA KR300, Comau NJ 650-2.7 (high-payload), and ABB IRB 4400 (low-payload), which differ in size, payload, and reach (Table 1, Figure 2). Table 1 shows that the three robots have different rated joint speeds and physical properties. The FRF experiments were performed with the robots at rest in fixed postures; therefore, the A1–A6 speed limits do not directly affect the small-amplitude vibration response measured. The main sources of variation across platforms are mass/inertia, link geometry, joint/gear stiffness and damping, and the controller's holding behavior, which affect the effective mass, damping, and stiffness of the system. These robots were intentionally chosen to evaluate the effectiveness of transfer learning and its ability to generalize from one robot model to structurally different robots with different vibration behavior, demonstrating the approach's scalability both upward and downward. For Robot A, over 250 hammer tests had already been performed in various postures, striking the end-effector in X, Y, and Z directions and recording vibrations with accelerometers [69].

Table 1. Characteristics of Robot A (KUKA KR300), Robot B (Comau NJ 650-2.7), and Robot C (ABB IRB 4400).

	KUKA KR300	**Comau NJ 650-2.7**	**ABB IRB 4400**
Maximum reach	3095 mm	2703 mm	1950 mm
Rated payload	300 kg	650 kg	60 kg
Number of axes	6	6	6
Mounting position	Floor	Floor	Floor
Repeatability	±0.06 mm	0.15 mm	±0.07 mm
Weight	approx. 1092 kg	2450 kg	1040 kg
Motion (range) speed A1	±185° (123°/s)	±180° (75°/s)	±165° (150°/s)
Motion (range) speed A2	−140°/−5° (115°/s)	−60°/75° (75°/s)	+96° to −70° (120°/s)
Motion (range) speed A3	−120°/155° (120°/s)	−231°/−10° (75°/s)	+65° to −60° (120°/s)
Motion (range) speed A4	±350° (292°/s)	±2700° (90°/s)	±200° (225°/s)
Motion (range) speed A5	±125° (258°/s)	±125° (90°/s)	±120° (250°/s)
Motion (range) speed A6	±350° (284°/s)	±2700° (120°/s)	±400° (330°/s)

It is noted that the KUKA KR300 robot was manufactured by KUKA Roboter GmbH, located in Augsburg, Germany. The Comau NJ 650-2.7 robot was produced by Comau S.p.A., based in Turin, Italy and the ABB IRB 4400 robot was made by ABB Robotics AB, part of ABB Ltd, headquartered in Zürich, Switzerland. These robots were sourced from well-established international manufacturers known for their advanced industrial automation technologies.

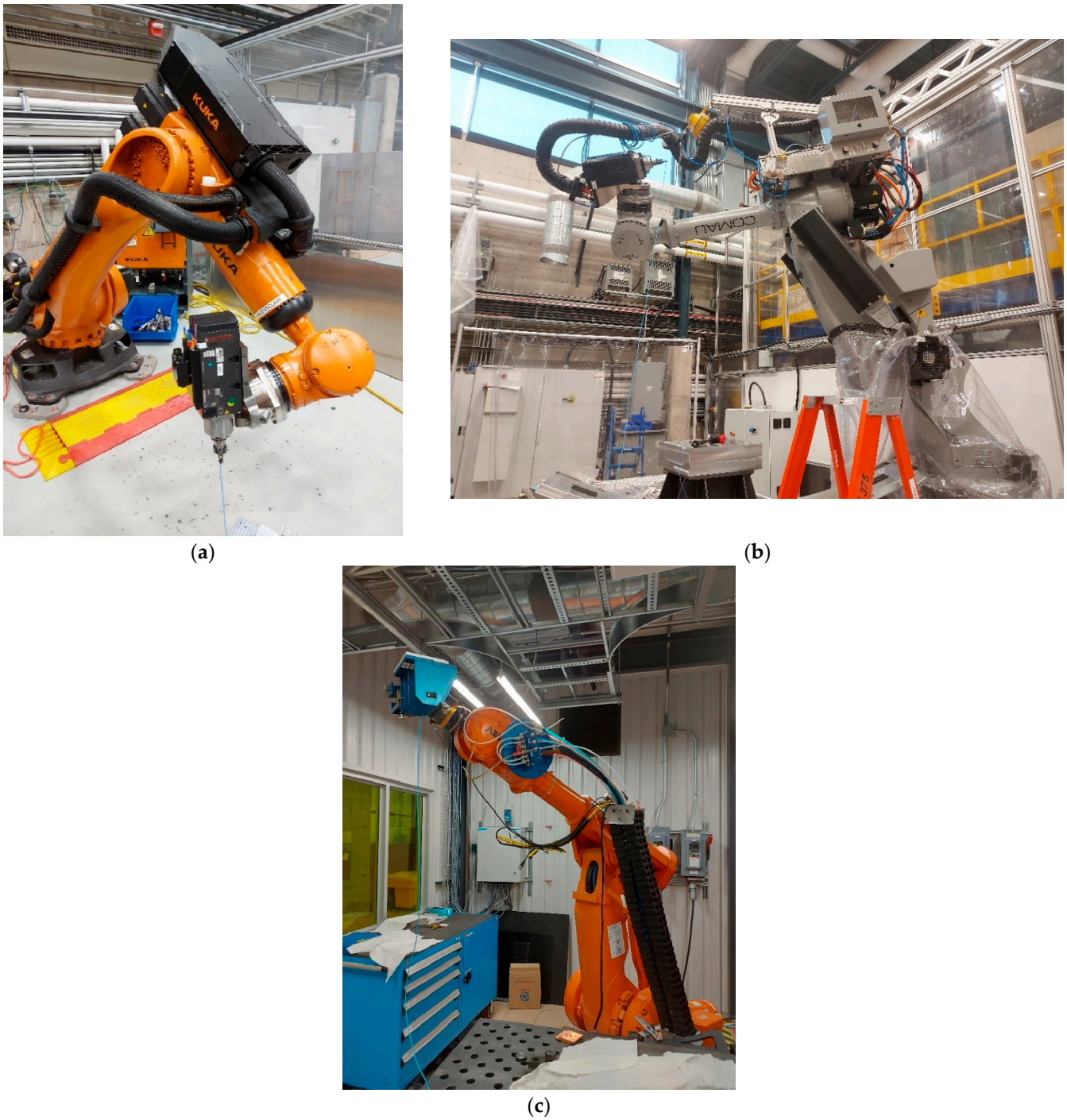

Figure 2. (**a**) The KUKA KR300 robot manipulator; (**b**) Comau NJ 650-2.7 robot manipulator; (**c**) ABB IRB 4400 robot manipulator.

For this study, new experiments with a reduced number of tests (robot configurations) were designed for two robot candidates: Robot B and Robot C, in alignment with the study's objective to minimize testing time and effort. Accordingly, only 25 postures were selected for Robot B and 29 (25 + 4) for Robot C to perform the hammer test. These limited tests were designed to evaluate whether transfer learning, using the knowledge learned from Robot A, can be used to predict the behavior of Robot B and Robot C using only a small amount of new data. The goal is to assess whether accurate predictions could be made with minimal testing. Table 2 presents the range of motion for each joint of Robots A, B, and C. All selected robot postures were verified in RoboDK software (version v5.9.1)

to ensure their feasibility in terms of reachability, joint limits, and collision avoidance (Figure 3). In the Comau NJ 650-2.7, the parallelogram linkage is equivalent to a 5-bar parallel mechanism, with the two actuated joints being on the same axis of rotation. As shown in Figure 4, the motors actuating Joint 2 and Joint 3 are coaxial. In Figure 4a, actuating Joint 2 while keeping Joint 3 constant, moves the link highlighted in light red. This changes the shape of the parallelogram and, consequently, the rotation limits of Joint 3, due to the mechanical constraints. The inverse effect occurs when actuating Joint 3 (Figure 4b—moving the link highlighted in light red), which affects the limits of Joint 2. Therefore, depending on whether the parallelogram is flattened or square, the allowable limits for both θ_2 and θ_3 vary. This coupling must be considered when defining valid robot postures, as ignoring it can lead to configurations outside the robot's mechanical range.

Table 2. Range of motion for each joint of Robots A, B, and C.

Axis	Motion Range		
	Robot A	**Robot B**	**Robot C**
Joint 1 (θ_1)	-50° to 50°	-60° to 87°	-59° to 47°
Joint 2 (θ_2)	-50° to -90°	-28° to 56°	-10° to 48°
Joint 3 (θ_3)	70° to 150°	-127° to -16°	-30° to 79°
Joint 4 (θ_4)	-300° to 300°	-158° to 232°	-184° to 190°
Joint 5 (θ_5)	-90° to 90°	-93° to 124°	-116° to 114°
Joint 6 (θ_6)	-300° to 300°	-283° to 201°	-360° to 296°

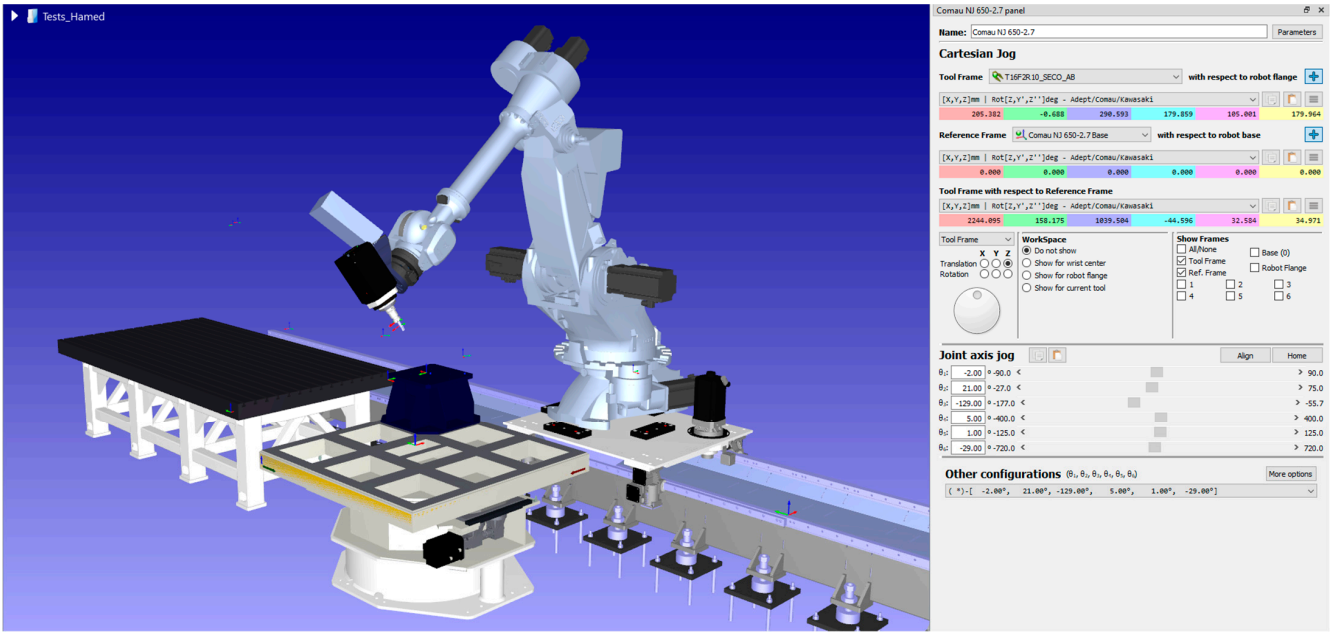

Figure 3. Posture validation of Comau NJ 650-2.7 robot manipulator using RoboDK simulation.

The vibration behavior at the tool center point (TCP) is critical because it directly affects machining quality, chatter, and process stability. For this reason, a triaxial accelerometer was mounted on the tool as close as possible to the TCP and oriented with the TCP axes so that the measured directions matched the excitation and response directions used in analysis and stability prediction. This position allowed vibration measurements in three directions (X, Y, and Z) and enabled accurate capture of the robot's dynamic response during hammer tests. Care was taken to ensure rigid mounting and proper cable management to avoid noise or measurement errors.

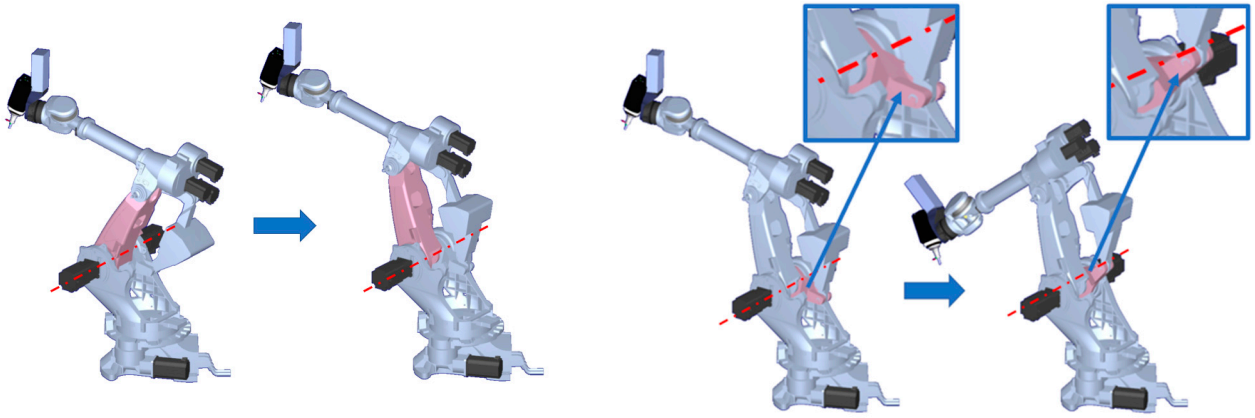

(**a**) (**b**)

Figure 4. Effect of parallelogram structure on joint motion in Comau NJ 650-2.7 (in each case, the link moved by the motor's joint is shown in light red). (**a**) Changing θ_2 while θ_3 is fixed reshapes the parallelogram and modifies the possible rotation range of θ_3 in both directions. (**b**) Changing θ_3 while θ_2 is fixed modifies the available rotation range of θ_2.

To perform the hammer tests, we used a set of precise measurement instruments. The setup included the LMS SCADAS Mobile data acquisition system connected to Siemens LMS Test.Lab software (Simcenter Testlab 2306) (Figure 5). A modal impact hammer (model 086D20) was used to excite the robot structure, and a triaxial accelerometer (model PCB HT356A43) was attached to the robot's tool (end-effector) to record vibration signals in three directions: X, Y, and Z. The acceleration data was sampled at 1024 Hz with a frequency resolution of 0.25 Hz. The time of collecting the signal for each test was 4 s, and the number of impacts per test was 5 to have a reliable signal. This setup ensured that we captured detailed information about the robot's dynamic behavior.

Figure 5. *Cont.*

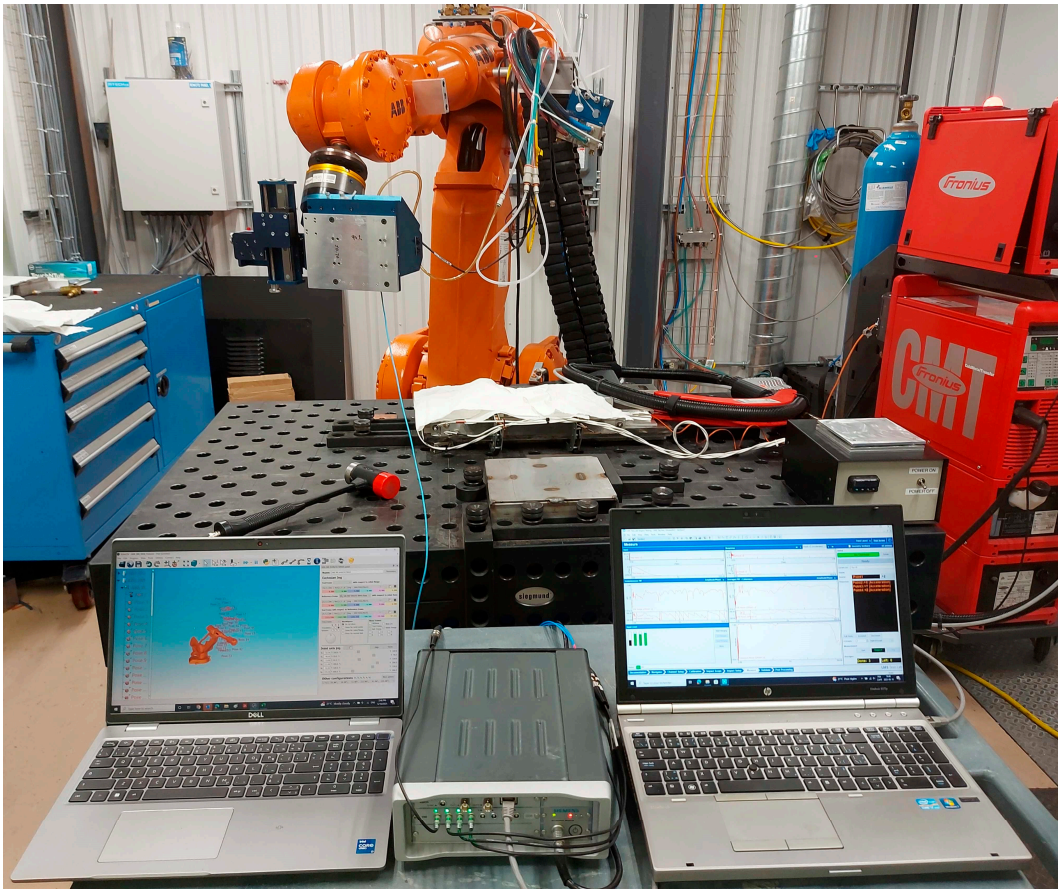

Figure 5. LMS SCADAS Mobile data acquisition system connected to Siemens LMS Test.Lab software.

2.2. Data Analysis and Post-Processing

Figure 6 shows some of the main challenges in selecting peaks from FRF data during modal analysis. In the first plot on the left, the FRF has many peaks, but it's hard to tell exactly how many real modes are present, maybe 13 or 14. This uncertainty makes it difficult to correctly identify modal parameters. In the second plot, it's unclear whether some of the small peaks are actual modes or just noise. This can cause errors if noise is mistakenly selected as a mode during analysis.

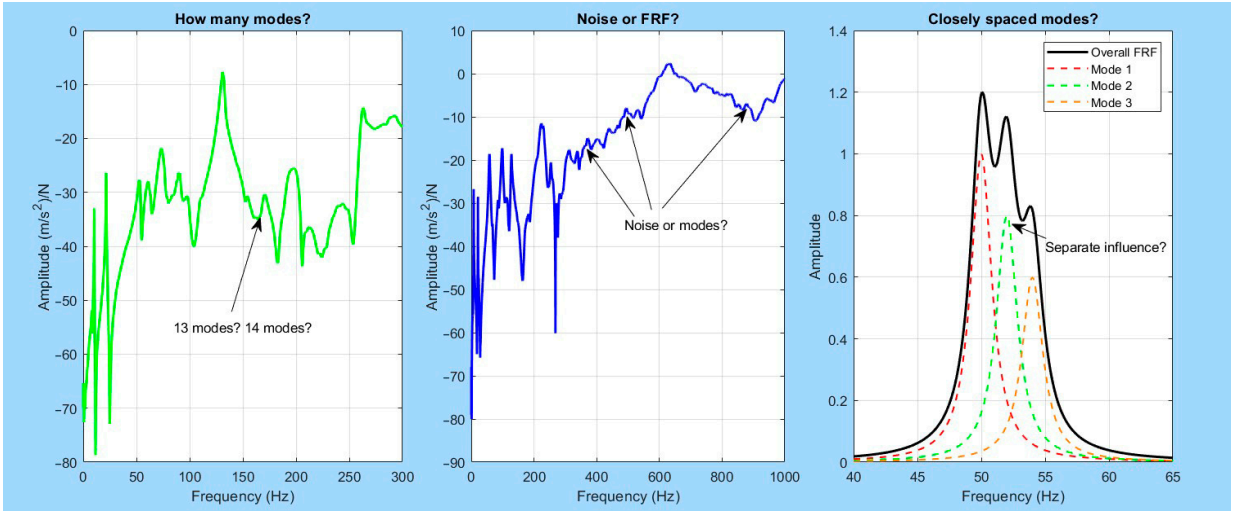

Figure 6. Illustration of challenges in modal parameter estimation from FRF Data.

The third plot shows another common issue: closely spaced modes. Here, multiple modes overlap and create one large peak in the overall FRF. This issue was observed in the FRFs obtained from the hammer tests conducted on the Comau robot. This makes it hard to separate their individual effects. If these modes are not clearly separated, the modal parameters (like natural frequency and damping) may not be estimated correctly. Figure 6 highlights the importance of careful data post-processing, including filtering, using stabilization diagrams, and expert judgment, to make accurate decisions about which peaks represent real modes.

To deal with the problems shown in Figure 6, like not knowing how many peaks are real, confusing noise with modes, or having peaks that are too close together, we needed a careful method for peak selection. Looking at the FRF curves by eye was a good first step, but it could sometimes lead to mistakes, especially when the data was noisy or complex. To make the process more accurate, we used a stabilization diagram after the manual step. This helped us check which peaks were real and stable, so we could be more confident in finding the correct modal parameters [69].

Before using the stabilization diagram, the first step in peak selection was manual inspection of the FRF curves. In this step, peaks were visually identified based on their sharpness, height, and spacing. This method was simple and useful, especially when the FRFs were clear and not too noisy. It allowed the user to focus on significant peaks that likely represent real modes quickly. However, manual selection had some disadvantages. It was time-consuming, depending on the user's experience, and could be affected by noise or closely spaced modes, leading to errors or missed peaks [69].

By comparing the FRFs from different postures that are close to each other, it becomes easier to identify real peaks and avoid missing important modes. Some peaks may look very small or almost hidden in one posture, but appear clearly in another. This happens because the accelerometer might be placed at a nodal point (where vibration is minimal) in one posture and at an anti-nodal point (where vibration is strong) in another [70]. Looking at multiple FRFs helps reduce the chance of mistaking noise for a real mode and gives a more complete picture of the system's behavior (Figure 7).

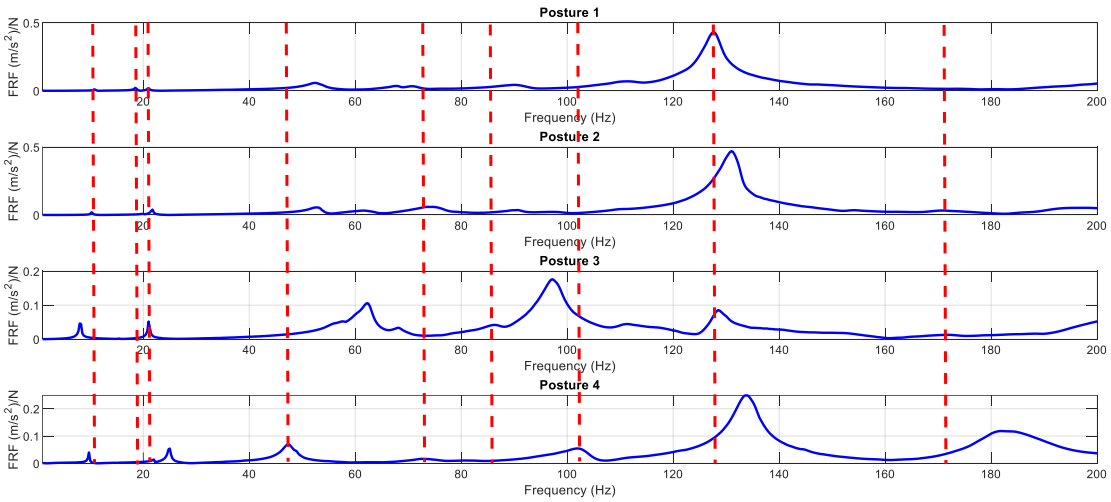

Figure 7. Comparison of FRFs from similar postures to improve peak identification and reduce noise influence.

To improve accuracy, the stabilization diagram was used after the manual step. This diagram helped confirm which peaks were real by showing how modal parameters (such as frequency and damping) changed as the model order increased. In the diagram, each point represented a possible mode, and stable modes appeared as vertical lines that remained

consistent across model orders. Unstable or false modes caused by noise usually disappear or shift position. By selecting only the stable poles, we could identify the correct modal parameters more reliably. Figure 8 shows the stabilization diagram from the LMS Test.Lab, where stable poles were marked and matched with the peaks in the FRF curve. This process reduced errors and increased confidence in the results.

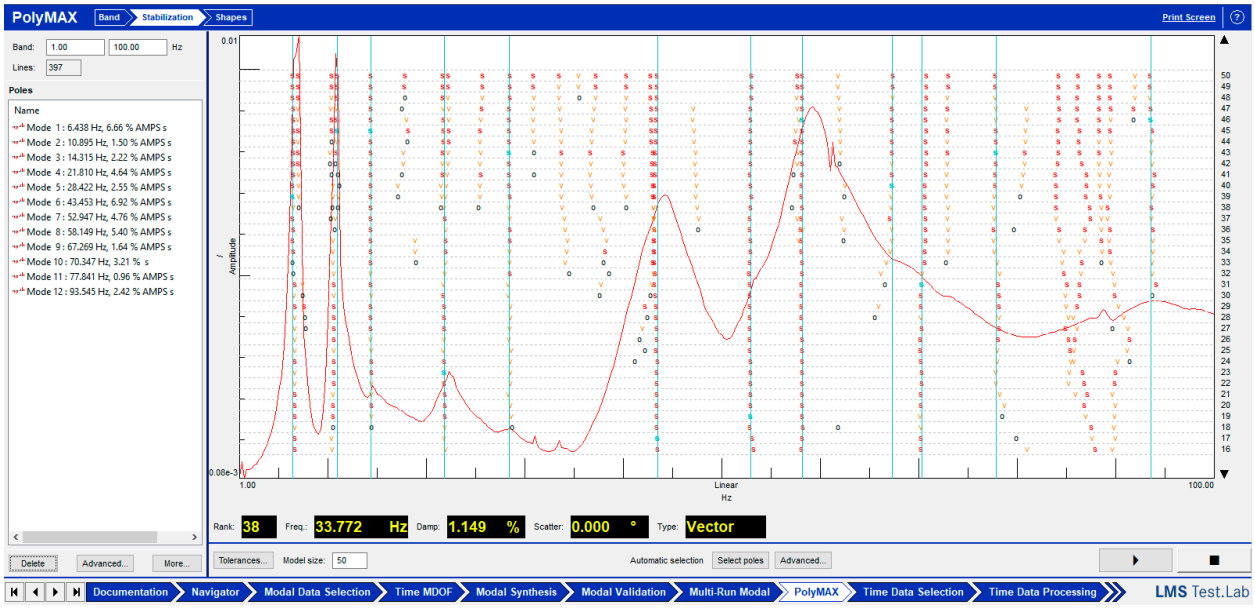

Figure 8. The stabilization diagram for the LMS PolyMAX® modal parameter identification software-assisted modal analysis, using measured FRFs.

In summary, after collecting the signals in the time domain, we used Fast Fourier Transform (FFT) and spectrum analysis to convert the data into the frequency domain in LMS software. The resulting FRFs were then post-processed to extract their vibration characteristics.

To further enhance accuracy, a special focus was given to identifying and validating the resonance peaks, as these peaks directly determine the natural frequencies and damping ratios of the robot. Modal assurance criteria (MAC) and repeated hammer tests were used to verify that the resonance peaks corresponded to consistent mode shapes across trials. Peaks that were unstable, shifted significantly between repeats, or failed MAC checks were discarded. By focusing on stable resonance peaks, we ensured that the final dataset contained only physically meaningful modes, reducing the influence of noise and spurious responses and providing a solid foundation for training predictive models.

After performing hammer tests and post-processing the data, datasets for different robots were prepared.

2.3. Deep Learning Framework Using Transfer Learning

Transfer learning is a method in machine learning where a model trained on one task is used to help with another similar task [71]. In this work, a deep learning approach was used to predict the vibration properties (like natural frequencies, damping ratios, and stiffness) of industrial robots. A relatively large dataset from Robot A (KUKA KR300) was used to train a predictive neural network for robot modal parameters in each configuration [69]. In this section, the methodology will be described for how to leverage this knowledge from Robot A to develop new prediction models for Robot B (Comau NJ 650-2.7) and Robot C (ABB IRB 4400), with significantly smaller datasets. This helps reduce the effort by requiring fewer tests and less data processing while still resulting in good prediction accuracy.

The deep learning model was built using Python 3.10. Different libraries, such as NumPy and Pandas, help manage the data, Matplotlib is used for visualizing results, and Scikit-learn is used for data scaling. The neural network itself is created using Keras, which is part of TensorFlow. These packages help prepare the data, train the model, and test its performance. To organize the datasets, file paths for different robots are stored in a dictionary called robot_configs, making it easy to switch between datasets for Robot A, B, or C. This setup makes the code clean, flexible, and easy to reuse for different robots.

A function called "process_data ( )" is responsible for loading the dataset from a CSV file and preparing it for training. First, it interpolates any missing values in the frequency response columns using linear interpolation. Then, it performs data augmentation by adding random noise (perturbation factor) to simulate variability and increased the dataset size. This is mathematically represented as:

$$X_{aug} = X + \epsilon \text{ where } \epsilon \sim \mathcal{U}(-\delta, \delta) \tag{1}$$

The perturbation factor δ controls the strength of the artificial noise added during data augmentation. In this study, $\delta = 0.10$ was chosen after testing different values (0.05, 0.10, 0.15) to balance realism and stability. This level of noise simulates small variations that can occur in practice, such as fluctuation in sensor readings or minor posture changes, without distorting the main resonance peaks of the FRFs. Generating multiple augmented samples increases model robustness, avoids overfitting, and improves generalization to unseen data. The data is then scaled between 0 and 1 to make learning easier and faster, using Min-Max normalization:

$$X_{\text{scaled}} = \frac{X - X_{min}}{X_{max} - X_{min}} \tag{2}$$

Finally, the data is split into training and test sets in an 80:20 ratio. Consequently, the function "build_model ( )" creates a deep neural network using Keras. The network has an input layer with six nodes (representing six joint angles), 5 hidden layers with 32 nodes each, and an output layer with 15 nodes (representing modal parameters). The activation function used in the hidden layers is ReLU (Rectified Linear Unit), defined as:

$$f(x) = max(0, x) \tag{3}$$

The model is compiled using the Adam optimizer and mean squared error (MSE) loss function:

$$MSE = \frac{1}{n}\sum_{i=1}^{n}(y_i - \hat{y}_i)^2 \tag{4}$$

This loss function penalizes large differences between predicted and true values.

- Transfer Learning

The predictive model of Robot A was previously trained on a relatively large dataset for over 500 epochs with a batch size of 8 (Figure 9).

Figure 9 shows the effect of batch size and number of epochs on the mean loss using repeated 5-fold cross-validation. The results indicate that smaller batch sizes improve learning stability, with the lowest loss achieved at a batch size of 8. Larger batch sizes led to higher loss, weaker gradient updates, and reduced generalization. Similarly, the epoch analysis shows that the loss decreases steadily up to around 500 epochs, after which the model begins to overfit and the loss increases. This confirms that 500 epochs provide the best balance between underfitting and overfitting, ensuring convergence without excessive

training. These results justify the choice of 500 epochs and a batch size of 8 as optimal for accurate and stable model performance.

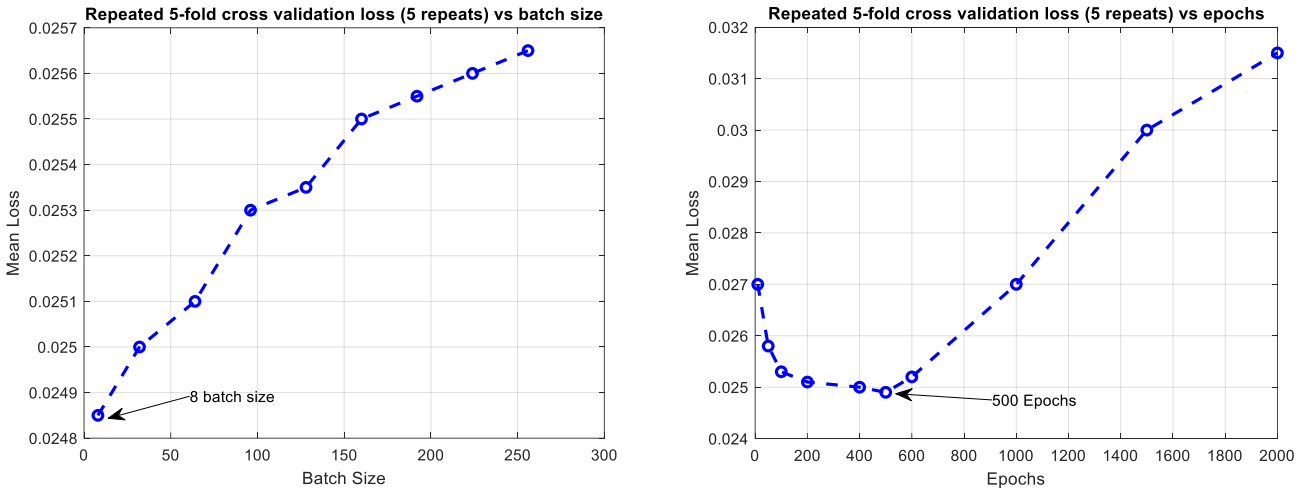

Figure 9. Effect of batch size (**left**) and number of epochs (**right**) on mean loss.

Now, the model is referred to here as the pretrained model, and it contains underlying relationship between robot joint angles and their corresponding modal parameters. Within the transfer learning framework, as illustrated in Figure 10, this relationship is adjusted to predict the modal parameters of Robot B and Robot C.

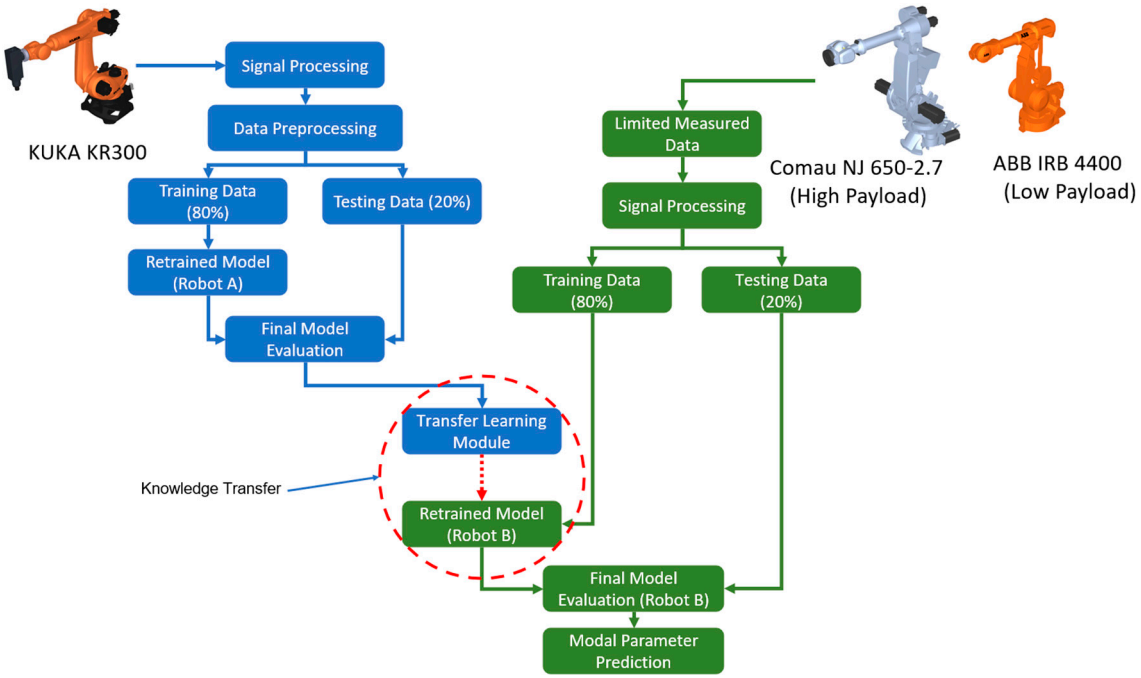

Figure 10. Transfer learning framework for modal parameter prediction from robot A (KUKA KR300) to robot B (Comau NJ 650-2.7) and Robot C (ABB IRB 4400).

For transfer learning to a new robot, the pretrained model is used partially, with some frozen layers, in our case, the first three layers. This helps preserve the learned features [72]. The remaining (trainable) layers are updated during training on the new robot's smaller dataset. This method works effectively when the new model is similar to the pretrained model but less data is available for training. It is important to note that the number of layers selected to remain frozen during transfer learning was chosen based on accuracy and

loss values observed during training. Selecting the appropriate number of frozen layers was determined through a trial-and-error process.

Figure 11 shows how transfer learning is used to build a deep learning model for Robot B using an already trained model from Robot A. At the top of the figure, the pretrained DNN for Robot A takes six robot joint angles as input (θ_1 to θ_6). This model has five hidden layers. The first three hidden layers (shown in blue) are already trained and contain important information about the robot's vibration behavior. These layers are called frozen, which means their weights do not change during training.

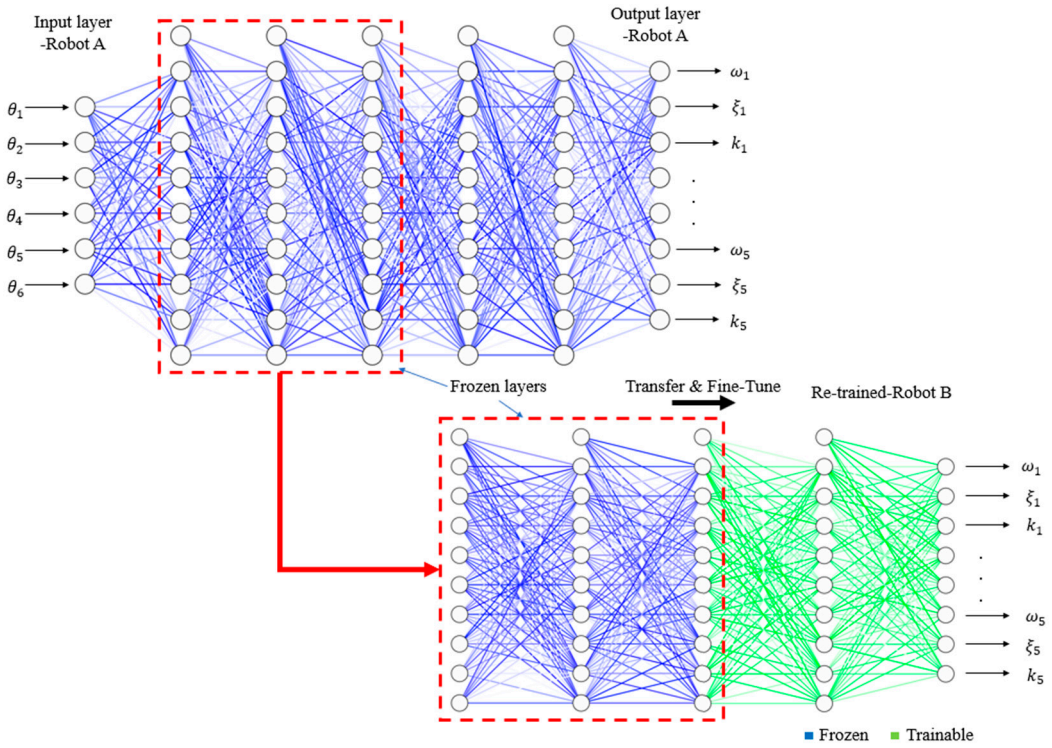

Figure 11. Transfer learning architecture from Robot A to Robot B using partially frozen deep neural network (DNN).

In the bottom part of Figure 11, the first three layers of the base model trained on Robot A are frozen and then reused to build a new model for Robot B. This step, indicated by the red arrow labeled "Transfer & Fine-Tune", ensures that the general features already learned from Robot A are preserved. These frozen layers capture low-level patterns of vibration and dynamic behavior, such as basic resonance trends, which are common across both robots and do not need to be relearned. After these frozen layers, two new trainable layers (shown in green) are added to the network. These layers remain adaptable and can update their weights to capture the posture-dependent and robot-specific behavior of Robot B.

During development, different freezing strategies were tested by locking 2, 3, or 4 layers. Freezing fewer than three layers led to excessive retraining, which caused overfitting to Robot B's limited dataset and poor generalization. Conversely, freezing more than three layers reduced network flexibility and restricted its ability to learn Robot B's unique vibration patterns. Freezing exactly three layers provided the most stable and accurate results, offering the best trade-off between preserving general vibration knowledge from Robot A and adapting to the new robot. This approach follows common practices in transfer learning, where early layers are kept fixed to retain general features, while later layers are fine-tuned for the target task.

As a result, the final transfer learning model for Robot B can predict modal parameters—including natural frequency (ω_n), damping ratio (ξ), and stiffness (k)—with both stability and accuracy. This balanced strategy leveraged the strengths of the original model while making the necessary adjustments to adapt to differences between robots.

2.4. Similarity Metrics: FRAC and NRMSE

To measure how well the predicted Frequency Response Functions (FRFs) match the experimental ones, two similarity metrics are used: the Frequency Response Assurance Criterion (FRAC) and the Normalized Root Mean Square Error (NRMSE) [73].

Frequency Response Assurance Criterion (FRAC):

FRAC is a correlation measure between two complex FRFs—the experimental FRF $H_{\text{exp}}(\omega)$ and the predicted FRF $H_{\text{pred}}(\omega)$. It evaluates how similar the two responses are in both magnitude and phase. FRAC values range from 0 (no correlation) to 1 (perfect correlation):

$$\text{FRAC} = \frac{\left|\sum_{\omega} H_{\text{pred}}(\omega) H^{*}_{\text{exp}}(\omega)\right|^2}{\left(\sum_{\omega} \left|H_{\text{pred}}(\omega)\right|^2\right)\left(\sum_{\omega} \left|H_{\text{exp}}(\omega)\right|^2\right)} \tag{5}$$

where $(\cdot)^*$ denotes the complex conjugate. FRAC values above 0.8 generally indicate good agreement.

Normalized Root Mean Square Error (NRMSE):

NRMSE compares the magnitudes of the predicted and the experimental FRFs, and is calculated as:

$$\text{NRMSE} = \frac{\left\|\left|H_{\text{pred}}(\omega)\right| - \left|H_{\text{exp}}(\omega)\right|\right\|}{\left\|\left|H_{\text{exp}}(\omega)\right|\right\|} \tag{6}$$

where $\|\cdot\|$ denotes the Euclidean norm. lower NRMSE values indicate closer agreement between prediction and measurement, with 0 representing a perfect match. In vibration studies, values below 0.3 are often considered acceptable.

3. Results and Discussion

This section presents and discusses the results of the proposed method for transferring a pretrained model for modal parameters prediction to new robots and estimating the FRFs of industrial robots.

First, the transfer learning approach, as presented in the previous section, is applied to the pretrained model with the limited dataset of Robot B to predict its modal parameters. The accuracy of the FRF estimation for Robot B is evaluated to demonstrate how well the predicted modal parameters capture the robot's vibration behavior.

Robot B has around twice the payload of Robot A. To further examine the effectiveness of the transfer learning method for a low-payload robot manipulator, the same approach was extended to Robot C, again using a small number of hammer tests. The performance of this new model was evaluated in predicting the modal parameters and estimating the FRFs of Robot C. For each robot, a comparison between the predicted and actual results was provided to assess the accuracy, reliability, and generalizability of the proposed method.

3.1. Results of Modal Prediction for Robot B

From 25 records of the Robot B datatest, 20 records were used for retraining the prediction model, and 5 were selected to evaluate the prediction accuracy. These postures were chosen to represent a range of joint configurations and to simulate a realistic low-data

scenario. The model was tasked with predicting modal parameters for these five new configurations using only joint angle data as input.

Figure 12 shows, in its first row, the plots of the training results for Robot A, the so-called pretrained model, as a reference. On the left, the accuracy plot shows how well the model learned during 500 training rounds (called epochs). We can see that both the training and validation accuracy steadily improved and reached around 90%, which means the model correctly predicted the output most of the time. On the right, the loss plot shows how much error the model made. The loss decreased quickly at the beginning and then slowly decreased further, showing that the model kept improving over time.

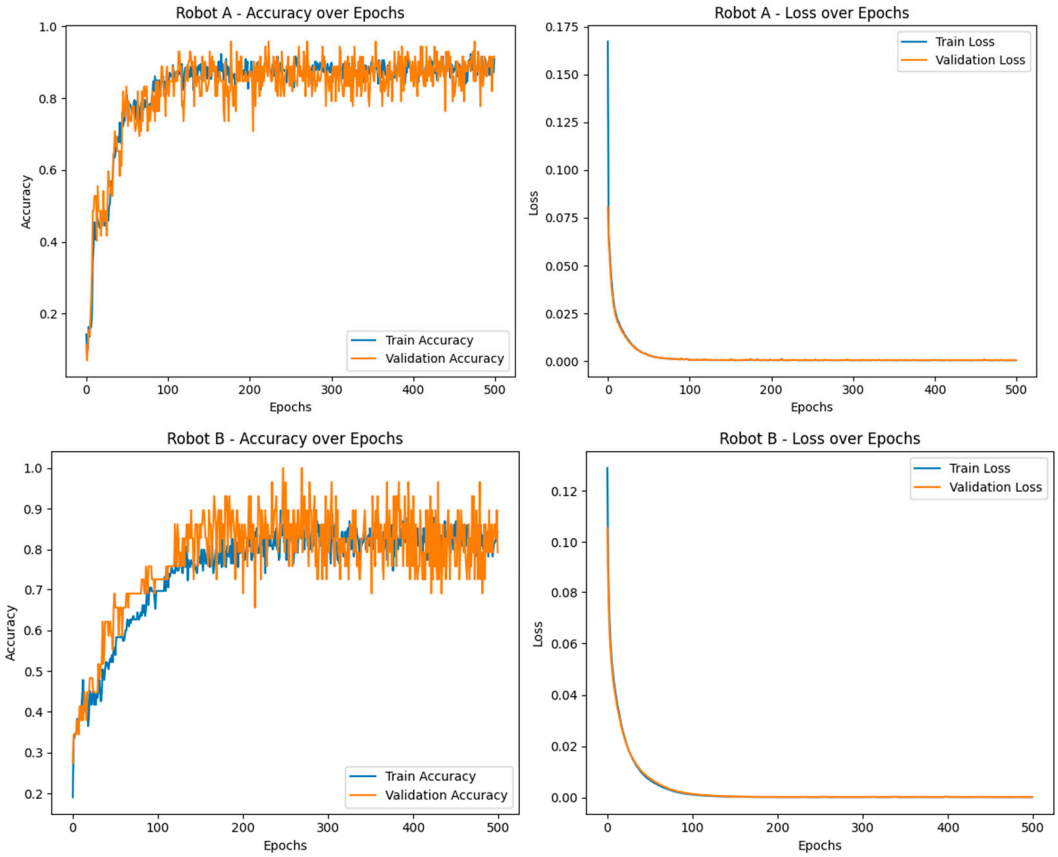

Figure 12. Training and validation performance of the transfer learning model for Robot A and Robot B: accuracy and loss over 500 epochs.

The second row of plots (Figure 12) shows the results after using transfer learning on Robot B, which had only a small amount of data (20 training tests). In the accuracy plot on the left, we can see that the model performed even better, with training and validation accuracy going above 85%. This means the model was very good at predicting the output for Robot B, even with fewer training samples. In the loss plot on the right, the error is very low, showing that the model predictions are close to the actual values. These results confirm that transfer learning achieved a good performance in using the knowledge of Robot A to predict the modal parameters of Robot B with a significantly smaller dataset.

Figure 13 shows the five selected postures of the Comau robot used for prediction. These postures are visually distinct and spread across the robot's working range. Table 3 lists the exact joint angles (in degrees) for all six joints of the robot in each posture. These postures were not part of the training data, so the results reflect the model's ability to generalize and predict unseen configurations.

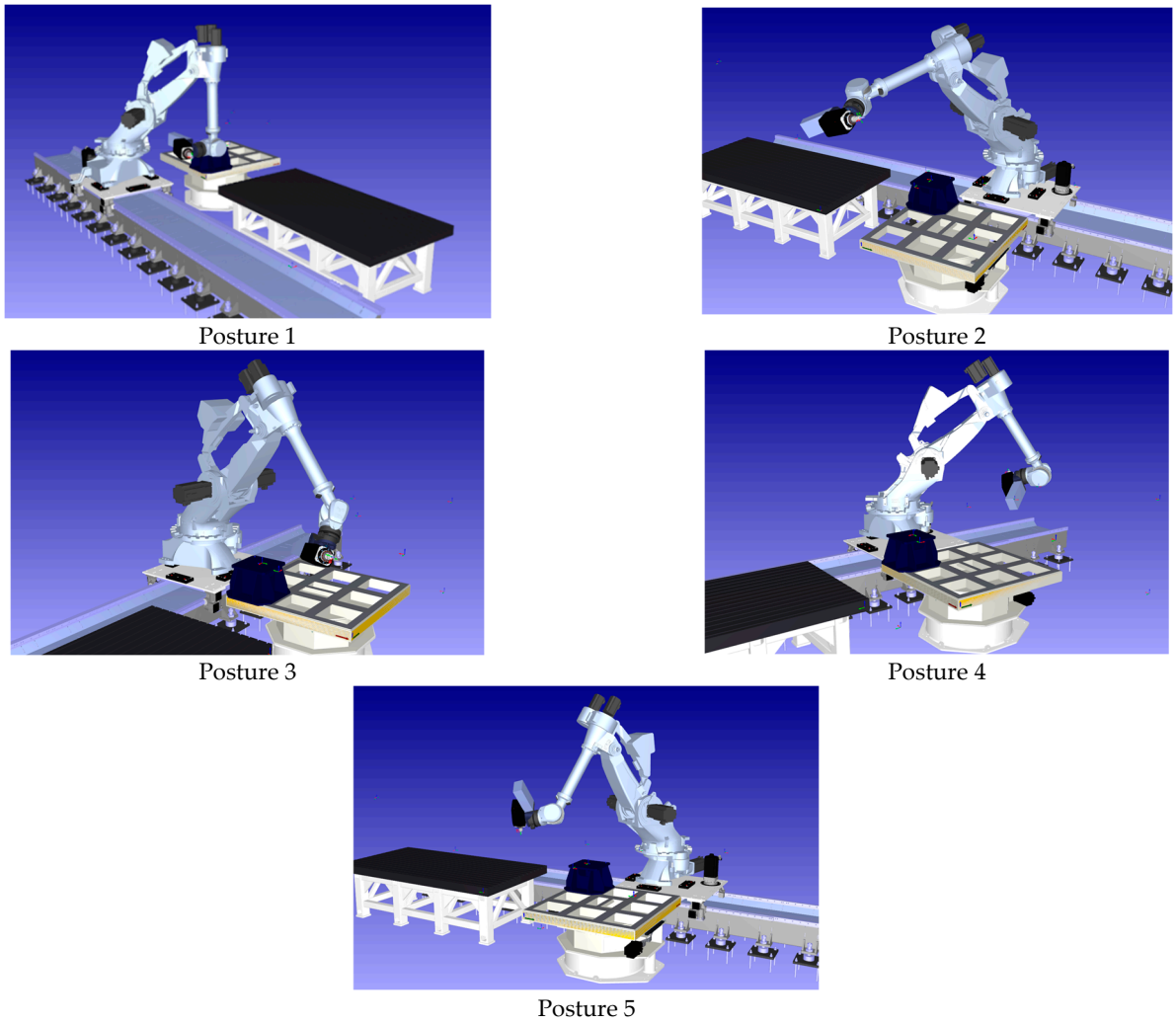

Figure 13. Selected postures of the Comau NJ 650-2.7 robot manipulator used for modal parameter prediction.

Table 3. Joint angles of the Comau robot (in degrees) for the five selected postures used in the testing phase.

Posture No.	Joint 1 (°)	Joint 2 (°)	Joint 3 (°)	Joint 4 (°)	Joint 5 (°)	Joint 6 (°)
1	−2	21	−27	5	1	−29
2	−60	50	−120	115	−66	−197
3	23	−28	−101	−82	124	168
4	59	51	−83	180	112	7
5	30	30	−102	−145	106	−11

Table 4 shows the comparison between the predicted modal parameters (using the TL model) and the experimental values (EMA) for three robot postures in the Y direction. The table includes three key modal parameters: natural frequency, damping ratio, and modal stiffness for the first five vibration modes. For each value, the table also shows the prediction error. As we can see, the predicted values are very close to the experimental ones, and the error percentages are small in most cases. This means the TL model is able to predict the dynamic behavior of the robot, making it useful when only a few experimental tests are available.

Table 4. The validation of modal parameters predicted by the proposed TL model and EMA for three distinct postures of Robot B.

Mode	**Posture 1**								
	Natural Frequency [Hz]			**Damping Ratio [%]**			**Modal Stiffness [10^5 N/m]**		
	EMA	**TL**	**%Error**	**EMA**	**TL**	**%Error**	**EMA**	**TL**	**%Error**
1	7.352	7.282	0.944	0.872	0.980	12.379	1.34682	1.35139	0.339
2	12.056	12.012	0.367	2.138	2.085	2.450	6.06784	6.19108	2.031
3	14.530	14.520	0.068	0.224	0.221	1.365	17.96839	18.20931	1.341
4	19.365	19.301	0.332	3.643	3.735	2.551	15.46110	15.32584	0.875
5	31.493	31.556	0.198	1.533	1.548	0.984	10.00344	9.93391	0.695
Mode	**Posture 2**								
	Natural Frequency [Hz]			**Damping Ratio [%]**			**Modal Stiffness [10^5 N/m]**		
	EMA	**TL**	**%Error**	**EMA**	**TL**	**%Error**	**EMA**	**TL**	**%Error**
1	6.965	7.020	0.803	1.020	1.046	2.582	1.32453	1.32285	0.127
2	11.263	11.239	0.210	0.407	0.482	18.354	0.74342	0.72240	2.828
3	14.730	14.806	0.515	6.895	6.817	1.133	4.56509	4.54101	0.527
4	23.769	23.832	0.265	2.334	2.442	4.656	26.90947	26.90342	0.022
5	30.273	30.278	0.017	2.932	2.954	0.761	14.55168	14.47240	0.545
Mode	**Posture 3**								
	Natural Frequency [Hz]			**Damping Ratio [%]**			**Modal Stiffness [10^5 N/m]**		
	EMA	**TL**	**%Error**	**EMA**	**TL**	**%Error**	**EMA**	**TL**	**%Error**
1	7.48	7.374	1.428	1.493	1.533	2.667	1.27141	1.28871	1.361
2	10.564	10.538	0.248	2.412	2.498	3.566	1.07695	1.20460	11.852
3	13.602	13.682	0.587	1.024	1.039	1.469	4.56509	4.52221	0.939
4	21.070	21.089	0.089	3.582	3.548	0.946	15.87799	15.95576	0.490
5	31.453	31.450	0.011	1.107	1.107	0.057	19.92689	19.97029	0.218

Figure 14 compares predicted and measured values for Robot B across five modes and five validation postures (Table 3) for three quantities: natural frequency, damping ratio, and modal stiffness. The predicted curves (dashed lines with squares) closely follow the real curves (solid lines with circles) in almost all cases, peaks line up, trends match, and levels are similar, with only small differences at a few points. Overall, the model estimates frequency, damping, and modal stiffness reliably for new robot postures.

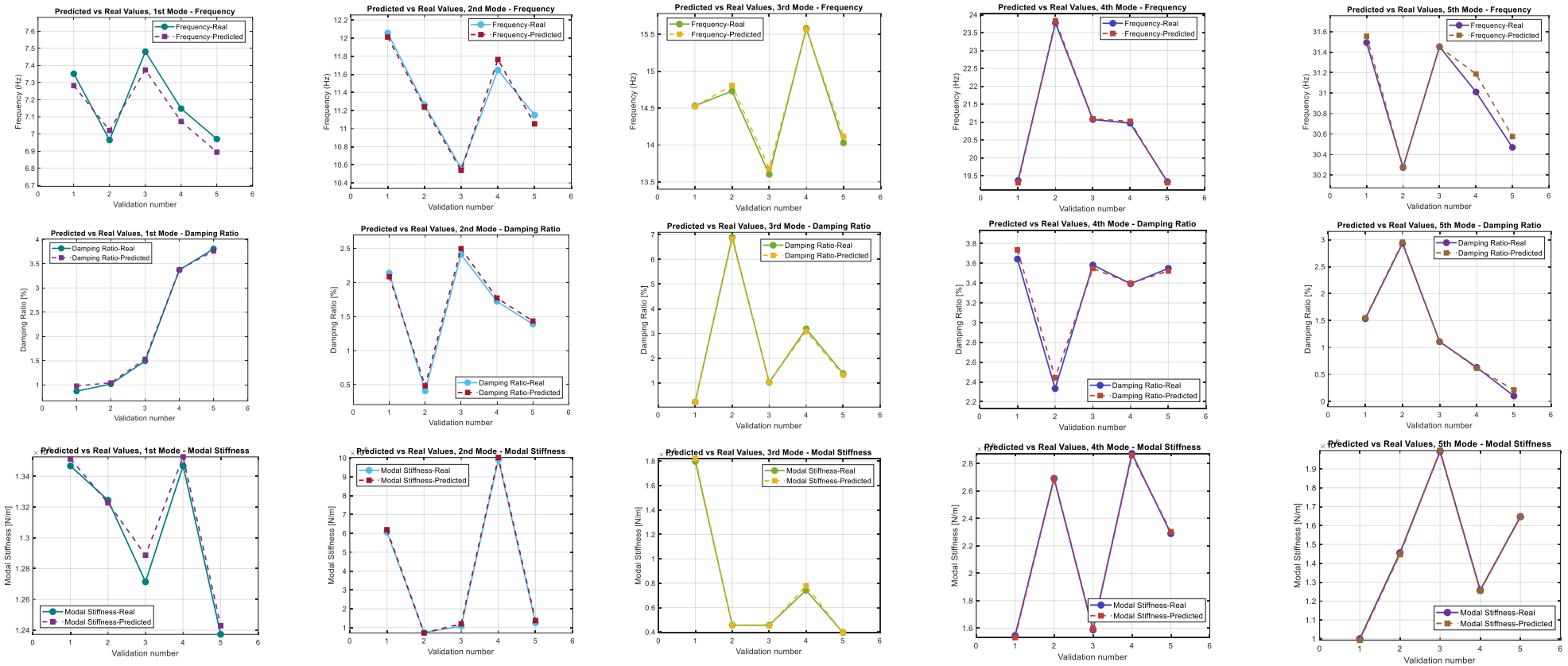

Figure 14. Predicted vs. real values of natural frequencies, damping ratios, and modal stiffnesses (modes 1–5) for Robot B.

3.2. Results of Modal Prediction for Robot C

The results of the retrained model for Robot C, applying the transfer learning approach, demonstrate the reliability of this method in applying learned knowledge about robot vibrations to different and distinct robots. For Robot C, we considered two significantly small datasets to assess the impact of varying training data sizes. The first dataset includes 20 records, while the second dataset is enhanced by adding 4 additional records to cover a more diverse range of joint configurations. This comparison highlights how dataset diversity affects the model's predictive accuracy and robustness.

The first row of plots in Figure 15 illustrates the training and validation performance of the transfer learning model for Robot C, based on an initial dataset of 20 records. These plots reveal that while the training accuracy and loss values of the new model are comparable to those of the pretrained model (first row of Figure 12), it struggles in validation with lower accuracy and higher loss values. This indicates that the model is limited in its ability to generalize effectively to unseen robot configurations. This limitation highlights the need for a more comprehensive dataset and further hammer tests to enhance the model's training data.

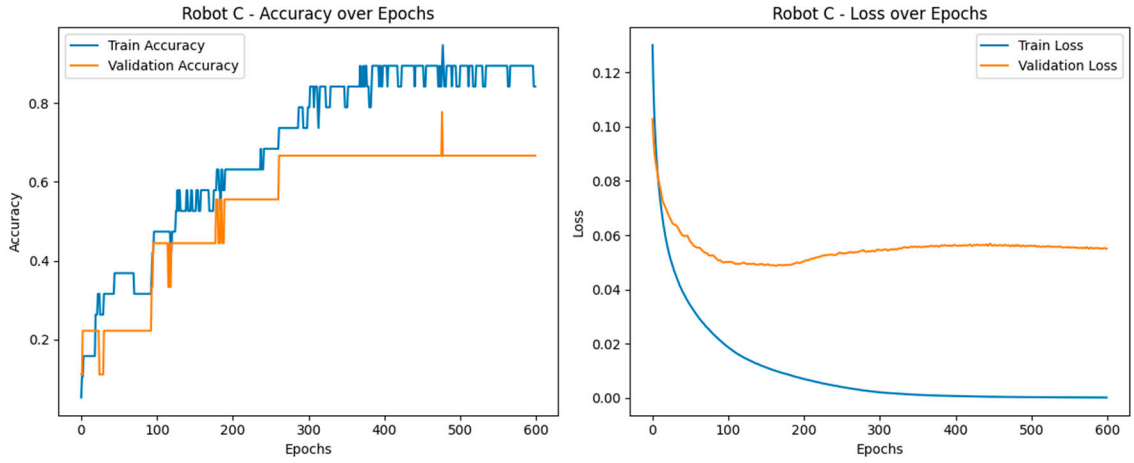

20 training tests

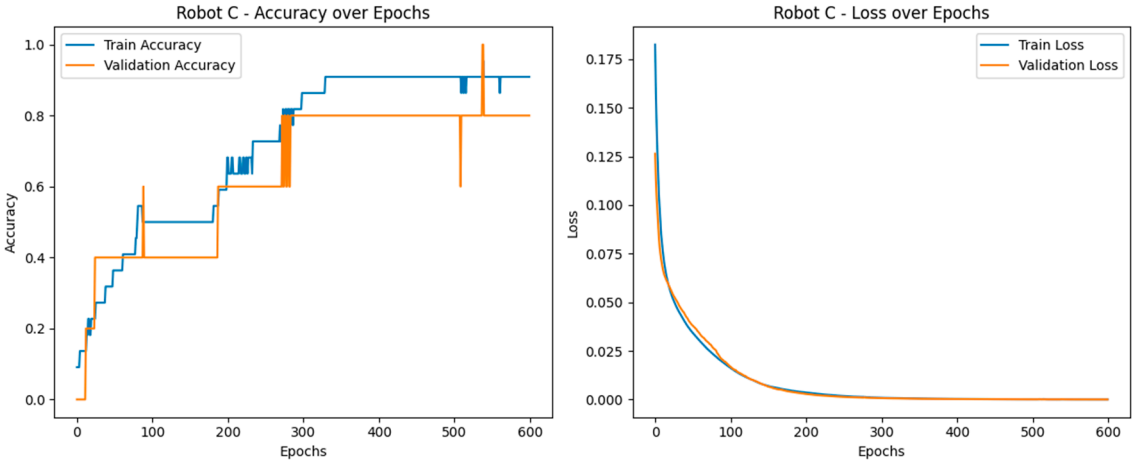

24 training tests

Figure 15. Training and validation performance of the transfer learning model for Robot C with 20 and 24 training tests.

The spatial distribution of the robot postures subjected to hammer tests and used for retraining is depicted in Figure 16. It was created using RoboDK. The left image shows that the initial 20 postures (Targets 1–20) were predominantly located on the robot's left

side, where many joint angles were negative. This unbalanced training set did not fully represent the robot's working range, which limited the model's ability to generalize and predict modal parameters accurately for all postures.

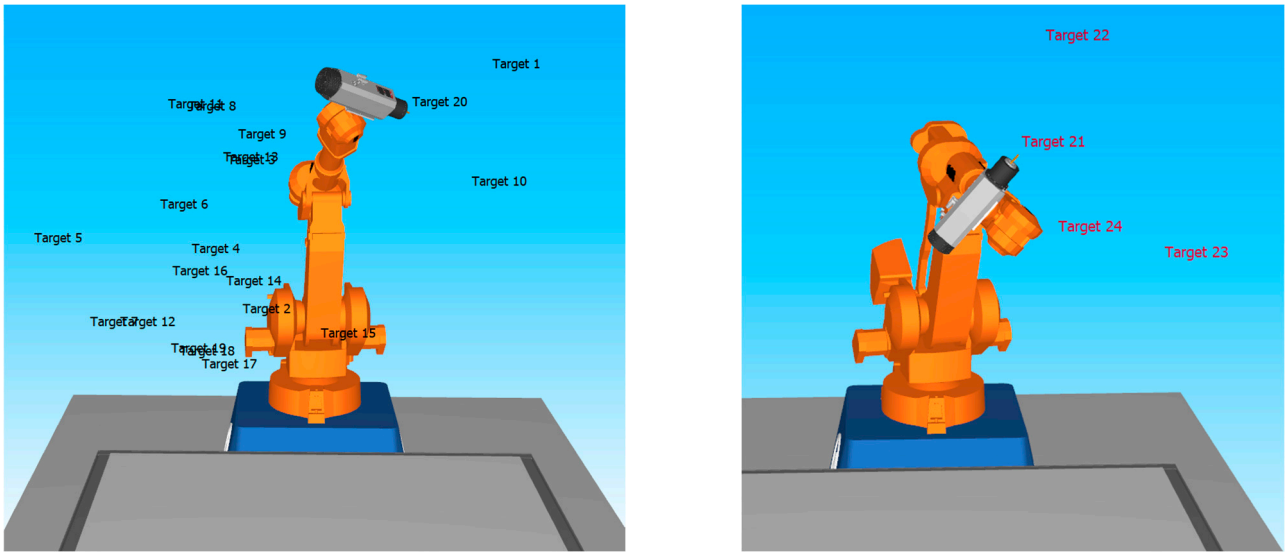

20 initial samples 24 samples (4 added samples)

Figure 16. Distribution of training postures in RoboDK: initial vs. added positions for improved accuracy.

To address this imbalance, four new postures were added for hammer testing, as indicated in red in the right image of Figure 16 (Targets 21–24). These additional postures were strategically placed on the right side of the robot and featured positive joint angles (Table 5). It resulted in a more balanced dataset with 24 records.

Table 5. Four added joint angles of the Robot C (in degrees) for the five selected postures used in the training phase.

Posture No.	Joint 1 (°)	Joint 2 (°)	Joint 3 (°)	Joint 4 (°)	Joint 5 (°)	Joint 6 (°)
21	12	26	9	50	−116	−286
22	23	6	−21	−117	−26	−37
23	32	36	35	143	46	−18
24	38	5	11	−92	114	152

Figure 17 compares the predicted and real natural frequencies for the 3rd and 5th vibration modes of Robot C, using two different training datasets: one with the initial dataset (20 tests) and another with the augmented and refined dataset (24 tests). With the initial dataset, the predicted values are sometimes far from the real values, especially for the 3rd mode, which shows larger prediction errors. With the augmented dataset, the predictions are much closer to the real values with better accuracy, as shown in the right-hand graphs of Figure 17. This proves that adding just a few extra training samples to complement the solution space can significantly improve the performance of the transfer learning model, especially in capturing the vibration behavior more precisely.

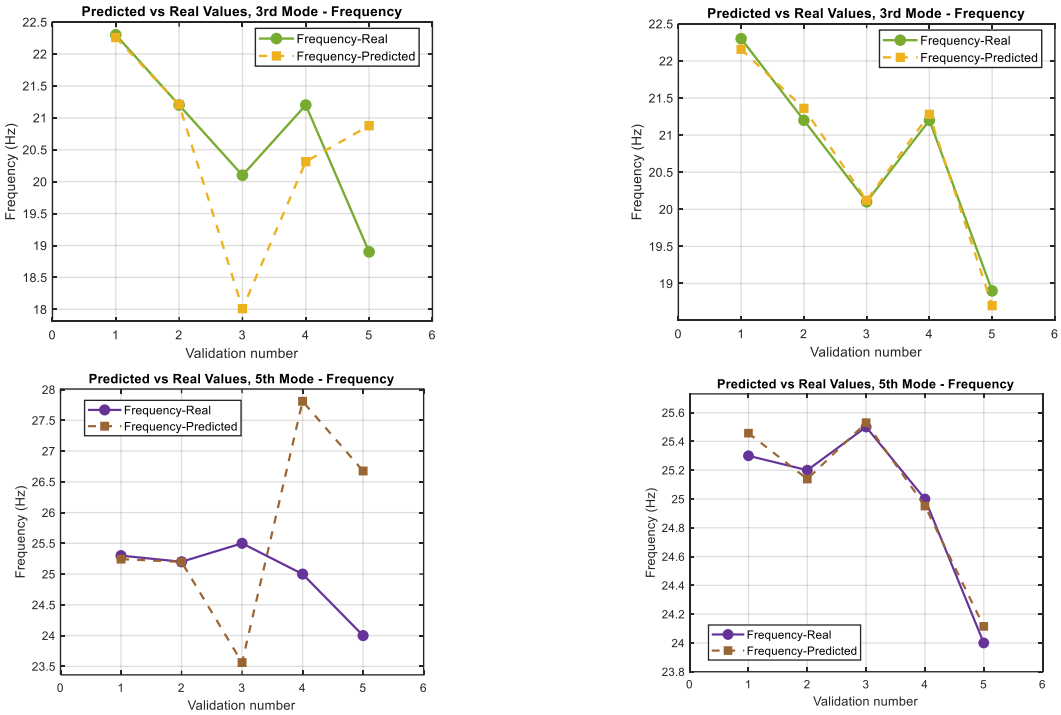

20 Training Tests 24 Training Tests (with 4 additional postures)

Figure 17. Effect of increasing training tests on frequency prediction accuracy for 3rd and 5th modes.

Now, five different postures of the Robot C were selected to test the prediction of modal parameters (Figure 18). These postures were chosen to represent various positions and movements of the robot arm. The joint angles for each of these five postures are shown in Table 6, where each row lists the angles (in degrees) for all six joints of the robot.

Table 6. Joint angles of the ABB robot (in degrees) for the five selected postures used in the testing phase.

Posture No.	Joint 1 (°)	Joint 2 (°)	Joint 3 (°)	Joint 4 (°)	Joint 5 (°)	Joint 6 (°)
1	39	8	8	98	−18	−30
2	47	−10	36	74	−89	−13
3	−3	48	20	−129	−57	−2
4	−2	20	−21	−167	−66	180
5	−6	−6	36	83	100	29

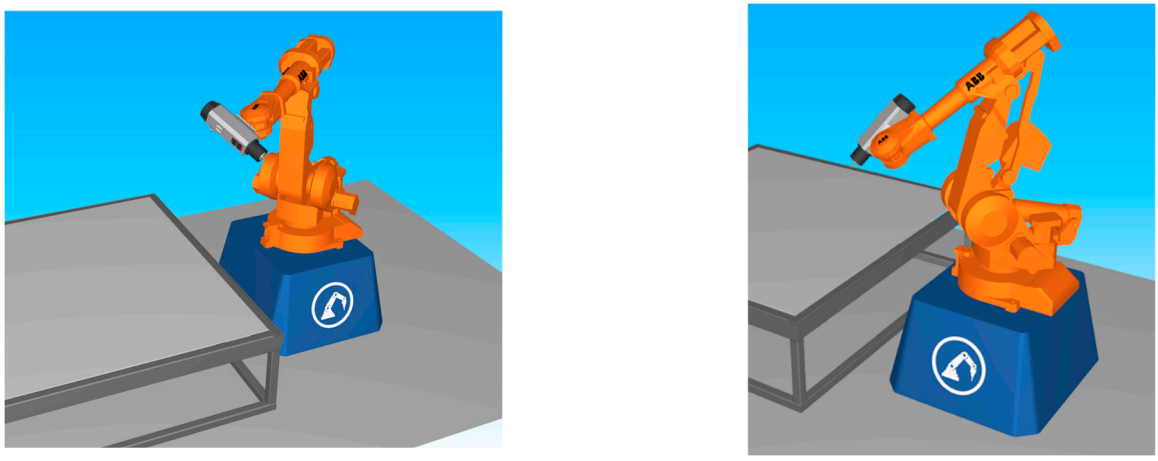

Posture 1 Posture 2

Figure 18. *Cont.*

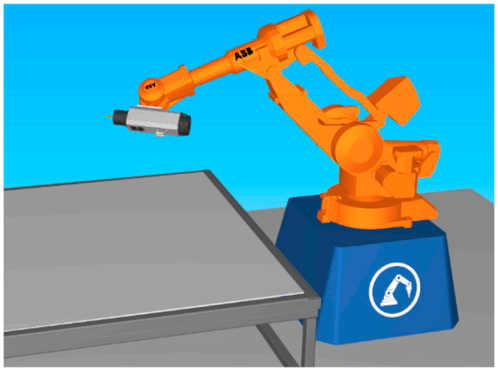

Posture 3

Posture 4

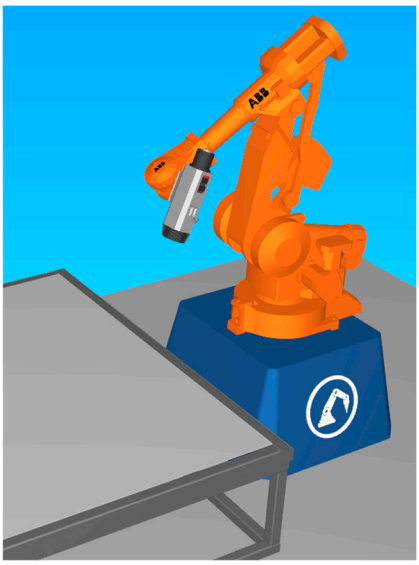

Posture 5

Figure 18. Selected postures of the ABB IRB 4400 robot manipulator used for modal parameter prediction.

The results in Figure 19 illustrate a comparison between the predicted and real values of the modal parameters for Robot C as a low-payload robot manipulator in five different modes. The predicted frequencies are very close to the real values in all modes. It shows that the model can correctly estimate the dynamic behavior of the robot with a refined dataset (24 training tests). Especially in the first and second modes, the predicted and real frequency values almost overlap. For higher modes (3 to 5), small differences can be seen, but the predicted curves still follow the same trend as the real data.

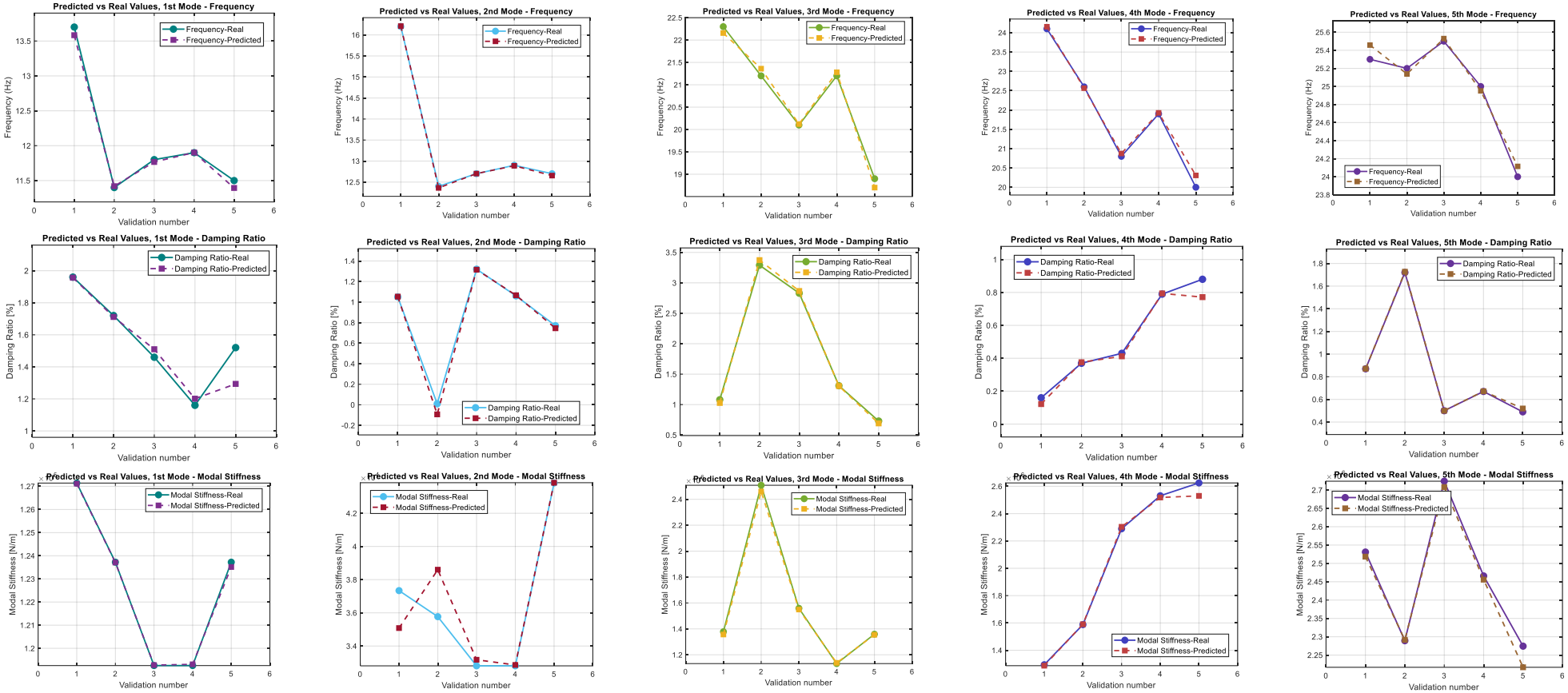

Figure 19. Predicted vs. real values of natural frequency, damping ratio, and modal stiffness (modes 1–5) for robot C.

For the damping ratio and modal stiffness, the predictions also match well with the real values. While some small errors appear in a few modes and validation points, the overall patterns are very similar. This means that the model can successfully predict how the robot behaves in terms of energy loss (damping) and stiffness.

Table 7 shows the comparison between the real values obtained from the EMA and the predicted values from the TL model for natural frequency, damping ratio, and modal stiffness across three different postures and five vibration modes of Robot C. The results demonstrate that the TL model predicts the modal parameters with high accuracy. Most of the errors are very small, typically less than 1% for natural frequency and modal stiffness, while damping ratio predictions show slightly higher errors in some cases, especially for Posture 1, Mode 4, and Posture 2, Mode 2. However, they remain within acceptable ranges.

Table 7. The validation of modal parameters predicted by the proposed TL model and EMA for three distinct postures of Robot C.

Mode	**Posture 1**								
	Natural Frequency [Hz]			**Damping Ratio [%]**			**Modal Stiffness [10^5 N/m]**		
	EMA	**TL**	**%Error**	**EMA**	**TL**	**%Error**	**EMA**	**TL**	**%Error**
1	13.7	13.5	0.851	1.960	1.957	0.171	1.27141	1.27116	0.019
2	16.2	16.21	0.064	1.050	1.053	0.277	0.37339	0.35082	6.043
3	22.3	22.1	0.642	1.080	1.027	4.947	13.78216	13.56449	1.579
4	24.1	24.15	0.224	0.160	0.122	23.85	12.94221	12.87258	0.538
5	25.3	25.45	0.622	0.870	0.871	0.084	25.30907	25.18429	0.493
Mode	**Posture 2**								
	Natural Frequency [Hz]			**Damping Ratio [%]**			**Modal Stiffness [10^5 N/m]**		
	EMA	**TL**	**%Error**	**EMA**	**TL**	**%Error**	**EMA**	**TL**	**%Error**
1	11.4	11.42	0.170	1.720	1.712	0.490	1.23723	1.23706	0.013
2	12.4	12.3	0.310	0.012	0.015	25.00	0.35768	0.38600	7.918
3	21.2	21.3	0.757	3.290	3.374	2.547	25.08313	24.60109	1.922
4	22.6	22.5	0.224	0.370	0.376	1.581	15.87798	12.87258	0.538
5	25.2	25.1	0.245	1.720	1.727	0.412	22.89233	22.91483	0.098
Mode	**Posture 3**								
	Natural Frequency [Hz]			**Damping Ratio [%]**			**Modal Stiffness [10^5 N/m]**		
	EMA	**TL**	**%Error**	**EMA**	**TL**	**%Error**	**EMA**	**TL**	**%Error**
1	11.8	11.7	0.282	1.460	1.510	3.418	1.19254	1.19275	0.017
2	12.7	12.702	0.012	1.320	1.315	0.374	0.32806	0.33172	1.118
3	20.1	20.122	0.108	2.830	2.866	1.290	15.58686	15.49222	0.607
4	20.8	20.87	0.361	0.430	0.412	4.167	22.89233	23.03473	0.622
5	25.5	25.53	0.118	0.500	0.500	0.005	27.24097	27.08077	0.588

The prediction errors for the damping ratio were larger than those for the natural frequency and modal stiffness, as shown in Tables 5 and 7 for Robots B and C. This trend is consistent with observations in mechanical and robotic systems, where the damping ratio is inherently more sensitive to uncertainties. Factors such as joint compliance, friction, nonlinear stiffness, and control dynamics strongly influence damping and make it less stable compared to natural frequency or stiffness. In addition, damping is highly affected by measurement noise, which further complicates accurate estimation. Therefore, the higher discrepancies observed in damping ratio predictions are not unexpected and reflect the well-known challenges of damping identification in complex robotic manipulators.

3.3. FRF Estimation for Robots B and C

The method for finding the relationship between the FRF and the equation of motion was explained in the work by Hosseini et al. [69]. In that study, formulas are provided to show how the FRF depends on modal parameters. These include the natural frequency (ω_n) and damping ratio (ξ), which are very important in describing how a system responds to vibrations. Using these formulas, the FRF can be estimated based on the predicted modal parameters.

Figure 20 compares the experimental (blue) and predicted (red dashed) FRF magnitude and phase for three postures of Robot B (high-payload) and Robot C (low-payload). Across all postures, the predicted curves closely follow the measured ones in the range of 0–40 Hz. Resonance peaks occur at nearly the same frequencies and with similar amplitudes, and the phase jumps near those peaks are well reproduced. The modal-frequency markers (• = experimental, × = predicted) align closely, confirming accurate parameter estimates. Small differences appear in the high-frequency tails.

To evaluate the similarity between experimental and predicted FRFs, as described in Section 2.4, two metrics were used: FRAC and NRMSE. FRAC is a complex correlation measure that quantifies the shape similarity of two FRFs and ranges between 0 and 1, with values close to 1 indicating strong agreement [73]. NRMSE is defined as the root mean square error between the magnitudes of the experimental and predicted FRFs, normalized by the magnitude of the experimental FRF; values approaching 0 indicates better accuracy. In practice, FRAC values above 0.8 and NRMSE values below 0.3 are generally interpreted as evidence of a reliable match between two FRFs. In this study, the reported FRAC values ($\approx$0.86–0.99) and NRMSE values ($\approx$0.03–0.32) confirm that the predicted FRFs align closely with the experimental ones across different postures.

In summary, the results show that transfer learning can predict robot modal parameters with minimal data. 20 training tests for Robot B and 24 for Robot C were enough to match measurements across five modes and multiple postures, with FRFs rebuilt from predictions showing high FRAC and low NRMSE. The key factor is data coverage of the workspace, not just data size. Robot C initially underperformed because its training postures were mostly on one side. Adding four targeted postures on the other side removed this bias and clearly improved accuracy. These findings confirm that the developed model generalizes well to both high-payload (Robot B) and low-payload (Robot C) manipulators, using only joint angles as inputs, and can reproduce their posture-dependent dynamics with reliable precision.

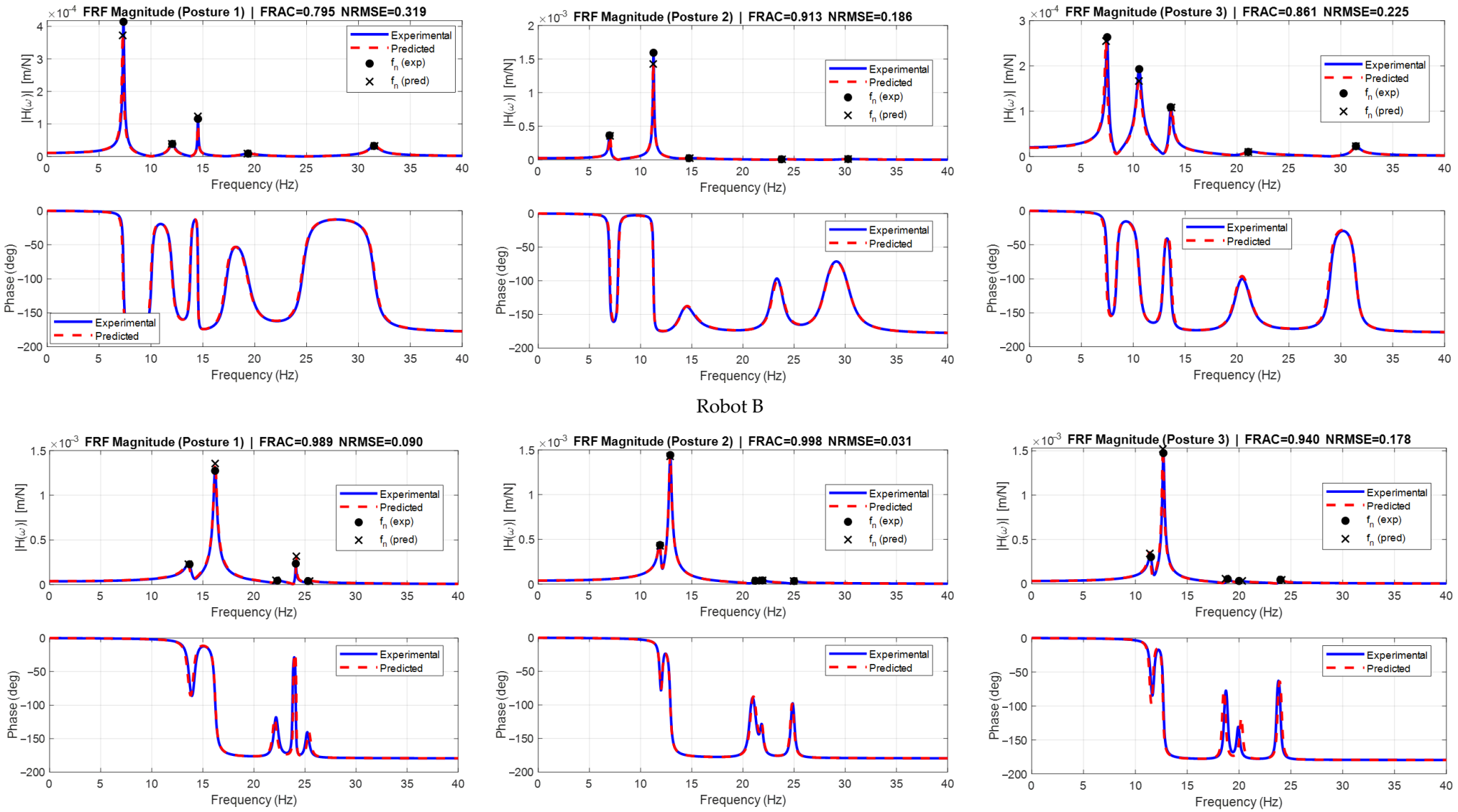

Figure 20. FRF Magnitude–Phase comparison across postures (experimental vs. predicted) for both robot B and C.

4. Conclusions

This study demonstrates that a deep learning (DL) model trained on Robot A can be extended to new robots using transfer learning (TL) with only a few hammer tests. The predicted modal parameters—natural frequencies (ω_n), damping ratios (ξ), and modal stiffness (k)—for Robot B (high-payload) and Robot C (low-payload) enabled accurate reconstruction of frequency response functions (FRFs), which closely matched experimental results with high Frequency Response Assurance Criterion (FRAC $\approx$ 0.86–0.99) and low Normalized Root Mean Square Error (NRMSE $\approx$ 0.03–0.32).

A key insight of this work is that data coverage is more important than dataset size. Robot C initially exhibited lower accuracy because its training postures were concentrated on one side of the workspace. By adding only four targeted postures from the opposite side, prediction accuracy improved, particularly for higher modes.

The novelty and main contributions of this research are: (1) applying DL with TL to posture-dependent vibration analysis of robots, (2) achieving accurate predictions with minimal experimental data, (3) demonstrating generalization across robots with different payload capacities, (4) reconstructing full FRFs from predicted modal parameters, and (5) showing that workspace coverage has a greater effect than dataset size.

Overall, the proposed TL framework provides a reliable and cost-effective approach to predict posture-dependent vibration behavior in industrial robots, reducing the need for extensive testing while maintaining high accuracy.

Author Contributions: S.H.S.H. led the research, including conceptualization, methodology, experimentation, data analysis, and manuscript drafting. S.H. and Z.L. supervised the research, contributed to the conceptualization and methodology, provided resources, and offered critical revisions and final approval of the manuscript. G.C. provided expert guidance during the experimental phase of the study. All authors have read and agreed to the published version of the manuscript.

Funding: This paper has been supported by (1) the National Research Council Canada (NRC) and (2) the Natural Sciences and Engineering Research Council of Canada (NSERC) through the Discovery Grants (Grant No. RGPIN-2019-05794 and RGPIN-2025-05609).

Data Availability Statement: The datasets presented in this article are not readily available because the data gathered from the robots used in this study are part of ongoing projects with clients. Providing open access to these datasets could inadvertently compromise client competitive advantage, as the data may contain proprietary information or insights that are integral to the clients' operational strategies. Additionally, premature release of this data might impact the integrity of the ongoing projects by exposing sensitive technical details that could be exploited by competitors. Therefore, to maintain the trust and confidentiality agreed upon with our clients, the data will remain embargoed. Requests to access the datasets should be directed to the corresponding author.

Acknowledgments: This work has been supported by the National Research Council Canada (NRC). The authors thank the NRC technical team, particularly the Robotics and Hybrid Manufacturing teams at the Aerospace Manufacturing Technologies Centre (AMTC). Furthermore, the financial support of the Natural Sciences and Engineering Research Council of Canada (NSERC) through the Discovery Grants is also acknowledged.

Conflicts of Interest: The authors declare no conflicts of interest.

References

1. Xin, S.; Tang, X.; Wu, J.; Peng, F.; Yan, R.; Yang, W. Investigation of the low-frequency chatter in robotic milling. *Int. J. Mach. Tools Manuf.* **2023**, *190*, 104048. [CrossRef]
2. Zhang, D.; Shao, S.; Zhao, X.; Zhou, C.; Liu, D.; Xu, P.; Kong, L. Advanced fault diagnostics in rotating machinery: A deep learning approach using octave theory of dynamic vibration signals. *J. Vib. Control* **2025**, *2025*, 10775463251314238. [CrossRef]

3. Espinoza-Sepulveda, N.; Sinha, J. Two-step vibration-based machine learning model for fault detection and diagnosis in rotating machine and its blind application. *Struct. Health Monit.* **2024**, *24*, 14759217241249055. [CrossRef]
4. Pan, X.; Zhang, X.; Jiang, Z.; Bin, G. Real-time intelligent diagnosis of co-frequency vibration faults in rotating machinery based on lightweight convolutional neural networks. *Chin. J. Mech. Eng.* **2024**, *37*, 41. [CrossRef]
5. Mendez, E.; Morán Ochoa, O.; Olivera-Guzman, D.; Soto-Herrera, V.H.; Luna-Sánchez, J.A.; Lucas-Dophe, C.; Lugo-del-Real, E.; Ayala-Garcia, I.N.; Alvarado Perez, M.; González, A. Integration of deep learning and collaborative robot for assembly tasks. *Appl. Sci.* **2024**, *14*, 839. [CrossRef]
6. Adebayo, R.; Obiuto, N.; Olajiga, O.; Festus-Ikhuoria, I.C. AI-enhanced manufacturing robotics: A review of applications and trends. *World J. Adv. Res. Rev.* **2024**, *21*, 2060–2072. [CrossRef]
7. Agrawal, B.P.; Sahoo, B.; Harini, V.; Lavanya, J.A.; Jindal, V.; Namdeo, A.K.; George, A.S. AI-driven robotics for real-time manufacturing processes. In *Role of Internet of Everything (IOE), VLSI Architecture, and AI in Real-Time Systems*; IGI Global Scientific Publishing: Hershey, PA, USA, 2024; pp. 199–212. [CrossRef]
8. Singh, M.; Liayakath, S.A.; Khan, A. Advances in autonomous robotics: Integrating AI and machine learning for enhanced automation and control in industrial applications. *Int. J. Multidimens. Res. Perspect.* **2024**, *2*, 74–90. [CrossRef]
9. Huang, Z.; Shen, Y.; Li, J.; Fey, M.; Brecher, C. A survey on AI-driven digital twins in Industry 4.0: Smart manufacturing and advanced robotics. *Sensors* **2021**, *21*, 6340. [CrossRef] [PubMed]
10. Petrone, V.; Ferrentino, E.; Chiacchio, P. On the role of artificial intelligence methods in modern force-controlled manufacturing robotic tasks. *arXiv* **2024**, arXiv:2409.16828. [CrossRef]
11. Eski, I.; Erkaya, S.; Savas, S.; Yildirim, S. Fault detection on robot manipulators using artificial neural networks. *Robot. Comput.-Integr. Manuf.* **2011**, *27*, 115–123. [CrossRef]
12. Liu, J.; Yang, X. Learning to see the vibration: A neural network for vibration frequency prediction. *Sensors* **2018**, *18*, 2530. [CrossRef]
13. Wang, S.; Shao, X.; Yang, L.; Liu, N. Deep learning aided dynamic parameter identification of 6-DOF robot manipulators. *IEEE Access* **2020**, *8*, 138102–138116. [CrossRef]
14. Reader, S.M.; Morand-Ferron, J.; Flynn, E. Animal and human innovation: Novel problems and novel solutions. *Philos. Trans. R. Soc. B Biol. Sci.* **2016**, *371*, 20150182. [CrossRef]
15. Barnett, S.M.; Ceci, S.J. When and where do we apply what we learn? A taxonomy for far transfer. *Psychol. Bull.* **2002**, *128*, 612–637. [CrossRef]
16. Schmidt, R.A.; Young, D.E. Transfer of movement control in motor skill learning. In *Transfer of Learning: Contemporary Research and Applications*; Cormier, S.M., Hagman, J.D., Eds.; Academic Press: Cambridge, MA, USA, 1987; pp. 47–79.
17. Xiang, Y.; Chen, F.; Wang, Q.; Gang, Y.; Zhang, X.; Zhu, X.; Liu, X.; Shao, L. Diff-transfer: Model-based robotic manipulation skill transfer via differentiable physics simulation. *arXiv* **2023**, arXiv:2310.04930.
18. Yang, Q.; Stork, J.A.; Stoyanov, T. Learn from robot: Transferring skills for diverse manipulation via cycle generative networks. In Proceedings of the 2023 IEEE 19th International Conference on Automation Science and Engineering (CASE), Auckland, New Zealand, 26–30 August 2023; pp. 1–6.
19. Chen, Y.; Jiang, J.; Lei, R.; Bekiroglu, Y.; Chen, F.; Li, M. GraspAda: Deep grasp adaptation through domain transfer. In Proceedings of the 2023 IEEE International Conference on Robotics and Automation (ICRA), London, UK, 29 May–2 June 2023; pp. 10268–10274.
20. Monorchio, L.; Capotondi, M.; Corsanici, M.; Villa, W.; De Luca, A.; Puja, F. Transfer and continual supervised learning for robotic grasping through grasping features. In *International Workshop on Continual Semi-Supervised Learning*; Springer: Cham, Switzerland, 2021; pp. 33–47.
21. Sun, L. Robot control policy transfer based on progressive neural network. In Proceedings of the 2023 IEEE 3rd International Conference on Information Technology, Big Data and Artificial Intelligence (ICIBA), Chongqing, China, 26–28 May 2023; Volume 3, pp. 1285–1289.
22. Scheiderer, C.; Mosbach, M.; Posada-Moreno, A.F.; Meisen, T. Transfer of hierarchical reinforcement learning structures for robotic manipulation tasks. In Proceedings of the 2020 International Conference on Computational Science and Computational Intelligence (CSCI), Las Vegas, NV, USA, 16–18 December 2020; pp. 504–509.
23. Guo, Y.; Jiang, Z.; Wang, Y.J.; Gao, J.; Chen, J. Decentralized motor skill learning for complex robotic systems. *IEEE Robot. Autom. Lett.* **2023**, *8*, 5791–5798. [CrossRef]
24. Cai, W.; Cheng, G.; Kong, L.; Dong, L.; Sun, C. Robust navigation with cross-modal fusion and knowledge transfer. In Proceedings of the 2023 IEEE International Conference on Robotics and Automation (ICRA), London, UK, 29 May–2 June 2023; pp. 10233–10239.
25. Van Baar, J.; Sullivan, A.; Cordorel, R.; Jha, D.; Romeres, D.; Nikovski, D. Sim-to-real transfer learning using robustified controllers in robotic tasks involving complex dynamics. In Proceedings of the 2019 International Conference on Robotics and Automation (ICRA), Montreal, QC, Canada, 20–24 May 2019; IEEE: Piscataway, NJ, USA, 2019; pp. 6001–6007.

26. Zhang, F.; Leitner, J.; Upcroft, B.; Corke, P. Vision-based reaching using modular deep networks: From simulation to the real world. *arXiv* **2016**, arXiv:1610.06781.
27. Kim, J.; Choi, S.; Kim, H.J. Fast and safe policy adaptation via alignment-based transfer. In Proceedings of the 2019 IEEE/RSJ International Conference on Intelligent Robots and Systems (IROS), Macau, China, 3–8 November 2019; pp. 990–996.
28. Yin, Z.; Ye, C.; An, H.; Lin, W.; Wang, Z. Robot manipulation skills transfer for sim-to-real in unstructured environments. *Electronics* **2023**, *12*, 411. [CrossRef]
29. Wernholt, E.; Gunnarsson, S. Analysis of methods for multivariable frequency response function estimation in closed loop. In Proceedings of the 2007 46th IEEE Conference on Decision and Control (CDC), New Orleans, LA, USA, 12–14 December 2007; pp. 4881–4888.
30. Schramm, L.; Sintov, A.; Boularias, A. Learning to transfer dynamic models of underactuated soft robotic hands. In Proceedings of the 2020 IEEE International Conference on Robotics and Automation (ICRA), Paris, France, 31 May–31 August 2020; pp. 4579–4585.
31. Lei, Y.; Hou, T.; Ding, Y. Prediction of the posture-dependent tool tip dynamics in robotic milling based on multi-task Gaussian process regressions. *Robot. Comput.-Integr. Manuf.* **2023**, *81*, 102508. [CrossRef]
32. Wang, R.; Li, F.; Niu, J.; Sun, Y. Prediction of pose-dependent modal properties and stability limits in robotic ball-end milling. *Robot. Comput.-Integr. Manuf.* **2022**, *75*, 102307. [CrossRef]
33. Chen, C.; Peng, F.; Yan, R.; Tang, X.; Li, Y.; Fan, Z. Rapid prediction of posture-dependent FRF of the tool tip in robotic milling. *Robot. Comput.-Integr. Manuf.* **2020**, *64*, 101906. [CrossRef]
34. Guihong, S.; Zhiqiang, L.; Yuchao, D.; Sichen, C.; Zirui, G.; Haoran, Z.; Xibin, W. Stability prediction for robotic milling based on tool tip frequency response prediction by considering the interface stiffness of spindle-tool system. *J. Sound Vib.* **2024**, *585*, 118471. [CrossRef]
35. Zimmermann, S.A.; Moberg, S. Experimental Evaluation of Methods for Estimating Frequency Response Functions of a 6-axes Robot. *arXiv* **2023**, arXiv:2312.06276. [CrossRef]
36. Ji, Y.; Liu, R. Research on the influence of cutter overhang length on robotic milling chatter stability. *Sci. Rep.* **2024**, *14*, 24838. [CrossRef] [PubMed]
37. Cordes, M.; Hintze, W.; Altintas, Y. Chatter stability in robotic milling. *Robot. Comput.-Integr. Manuf.* **2019**, *55*, 11–18. [CrossRef]
38. Hao, D.; Wang, W.; Liu, Z.; Yun, C. Experimental study of stability prediction for high-speed robotic milling of aluminum. *J. Vib. Control* **2020**, *26*, 387–398. [CrossRef]
39. Do, T.T.; Vu, V.H.; Liu, Z. Linearization of dynamic equations for vibration and modal analysis of flexible joint manipulators. *Mech. Mach. Theory* **2022**, *167*, 104516. [CrossRef]
40. Hosna, A.; Merry, E.; Gyalmo, J.; Alom, Z.; Aung, Z.; Azim, M.A. Transfer learning: A friendly introduction. *J. Big Data* **2022**, *9*, 102. [CrossRef]
41. Deng, Z.; Choi, K.S.; Jiang, Y.; Wang, S. Generalized hidden-mapping ridge regression, knowledge-leveraged inductive transfer learning for neural networks, fuzzy systems and kernel methods. *IEEE Trans. Cybern.* **2014**, *44*, 2585–2599. [CrossRef]
42. Kumari, S.; Singh, P. Deep learning for unsupervised domain adaptation in medical imaging: Recent advancements and future perspectives. *Comput. Biol. Med.* **2024**, *170*, 107912. [CrossRef]
43. Bahadori, M.T.; Liu, Y.; Zhang, D. Learning with minimum supervision: A general framework for transductive transfer learning. In Proceedings of the 2011 IEEE 11th International Conference on Data Mining, Vancouver, BC, Canada, 11–14 December 2011; IEEE: Piscataway, NJ, USA, 2011; pp. 61–70.
44. Bahadori, M.T.; Liu, Y.; Zhang, D. A general framework for scalable transductive transfer learning. *Knowl. Inf. Syst.* **2014**, *38*, 61–83. [CrossRef]
45. Rohrbach, M.; Ebert, S.; Schiele, B. Transfer learning in a transductive setting. *Adv. Neural Inf. Process. Syst.* **2013**, *1*, 46–54.
46. Quanz, B.; Huan, J. Large margin transductive transfer learning. In Proceedings of the 18th ACM Conference on Information and Knowledge Management, Hong Kong, China, 2–6 November 2009; pp. 1327–1336.
47. Wilson, G.; Cook, D.J. A survey of unsupervised deep domain adaptation. *ACM Trans. Intell. Syst. Technol. (TIST)* **2020**, *11*, 1–46. [CrossRef]
48. Yao, Z.; Wang, Y.; Long, M.; Wang, J. Unsupervised transfer learning for spatiotemporal predictive networks. In Proceedings of the International Conference on Machine Learning (PMLR), Vienna, Austria, 12–18 July 2020; pp. 10778–10788.
49. Zhang, Y.; Jiang, H.; Miura, Y.; Manning, C.D.; Langlotz, C.P. Contrastive learning of medical visual representations from paired images and text. In Proceedings of the Machine Learning for Healthcare Conference, Durham, UK, 5 August 2022; pp. 2–25.
50. Han, Z.; Sun, H.; Yin, Y. Learning transferable parameters for unsupervised domain adaptation. *IEEE Trans. Image Process.* **2022**, *31*, 6424–6439. [CrossRef]
51. Chang, H.; Han, J.; Zhong, C.; Snijders, A.M.; Mao, J.H. Unsupervised transfer learning via multi-scale convolutional sparse coding for biomedical applications. *IEEE Trans. Pattern Anal. Mach. Intell.* **2017**, *40*, 1182–1194. [CrossRef] [PubMed]

52. Mousavi, S.; Gagnol, V.; Bouzgarrou, B.C.; Ray, P. Stability optimization in robotic milling through the control of functional redundancies. *Robot. Comput.-Integr. Manuf.* **2018**, *50*, 181–192. [CrossRef]
53. Denkena, B.; Bergmann, B.; Reimer, S. Analysis of different machine learning algorithms to learn stability lobe diagrams. *Procedia CIRP* **2020**, *88*, 282–287. [CrossRef]
54. Li, M.; Huang, D.; Yang, X. Chatter stability prediction and detection during high-speed robotic milling process based on acoustic emission technique. *Int. J. Adv. Manuf. Technol.* **2021**, *117*, 1589–1599. [CrossRef]
55. Ikkache, K.; Chellil, A.; Lecheb, S.; Mechakra, H. Dynamic modeling of milling and effect of tool path on machining stability. *Int. J. Adv. Manuf. Technol.* **2022**, *121*, 1769–1783. [CrossRef]
56. Furtado, L.F.F.; Villani, E.; Trabasso, L.G.; Sutério, R. A method to improve the use of 6-dof robots as machine tools. *Int. J. Adv. Manuf. Technol.* **2017**, *92*, 2487–2502. [CrossRef]
57. Dong, X.; Qiu, Z. Stability analysis in milling process based on updated numerical integration method. *Mech. Syst. Signal Process.* **2020**, *137*, 106435. [CrossRef]
58. Peng, Y.; Li, B.; Mao, X.; Liu, H.; Qin, C.; He, H. A method to obtain the in-process FRF of a machine tool based on operational modal analysis and experiment modal analysis. *Int. J. Adv. Manuf. Technol.* **2018**, *95*, 3599–3607. [CrossRef]
59. Deng, K.; Gao, D.; Zhao, C.; Lu, Y. Prediction of in-process frequency response function and chatter stability considering pose and feedrate in robotic milling. *Robot. Comput.-Integr. Manuf.* **2023**, *82*, 102548. [CrossRef]
60. Tunc, L.T.; Gonul, B. Effect of quasi-static motion on the dynamics and stability of robotic milling. *CIRP Ann.* **2021**, *70*, 305–308. [CrossRef]
61. Mohammadi, Y.; Ahmadi, K. In-process frequency response function measurement for robotic milling. *Exp. Tech.* **2023**, *47*, 797–816. [CrossRef]
62. Chen, H.; Ahmadi, K. Estimating pose-dependent FRF in machining robots using multibody dynamics and Gaussian Process Regression. *Robot. Comput.-Integr. Manuf.* **2022**, *77*, 102354. [CrossRef]
63. Huynh, H.N.; Assadi, H.; Dambly, V.; Rivière-Lorphèvre, E.; Verlinden, O. Direct method for updating flexible multibody systems applied to a milling robot. *Robot. Comput.-Integr. Manuf.* **2021**, *68*, 102049. [CrossRef]
64. Jaquier, N.; Welle, M.C.; Gams, A.; Yao, K.; Fichera, B.; Billard, A.; Ude, A.; Asfour, T.; Kragic, D. Transfer learning in robotics: An upcoming breakthrough? A review of promises and challenges. *Int. J. Robot. Res.* **2024**, *44*, 465–485. [CrossRef]
65. Ahmed, O.; Träuble, F.; Goyal, A.; Neitz, A.; Bengio, Y.; Schölkopf, B.; Bauer, S.; Wüthrich, M. CausalWorld: A robotic manipulation benchmark for causal structure and transfer learning. *arXiv* **2020**, arXiv:2010.04296. [CrossRef]
66. Aitygulova, E.; Panov, A.I. Transfer learning with demonstration forgetting for robotic manipulator. *Procedia Comput. Sci.* **2021**, *186*, 374–380. [CrossRef]
67. Elci, H.; Longman, R.W.; Phan, M.Q.; Juang, J.-N.; Ugoletti, R. Discrete frequency-based learning control for precision motion control. In Proceedings of the Systems, Man and Cybernetics, San Antonio, TX, USA, 2–5 October 1994; Volume 3, pp. 2767–2773. [CrossRef]
68. Tang, H.; Notash, L. Neural network-based transfer learning of manipulator inverse displacement analysis. *J. Mech. Robot.* **2021**, *13*, 035004. [CrossRef]
69. Hosseini, S.H.S.; Hajzargarbashi, S.; Liu, Z. Enhancing robotic manipulator performance through analyzing vibration, identifying deep-learning-based modal parameters, and estimating frequency response functions. *Int. J. Adv. Manuf. Technol.* **2025**. [CrossRef]
70. Scheffer, C.; Girdhar, P. *Practical Machinery Vibration Analysis and Predictive Maintenance*; Elsevier: Amsterdam, The Netherlands, 2004.
71. Pan, S.J.; Yang, Q. A survey on transfer learning. *IEEE Trans. Knowl. Data Eng.* **2010**, *22*, 1345–1359. [CrossRef]
72. Zheng, M. The impact of decreasing dataset sizes on frozen layer transfer learning. *Sch. Rev. J.* **2021**, *2*. [CrossRef]
73. Ewins, D.J. *Modal Testing: Theory, Practice and Application*; John Wiley & Sons: Hoboken, NJ, USA, 2009.